SYNTHESIS AND CHARACTERIZATION OF VARIOUS COINAGE METAL COMPLEXES WITH BRIDGING DIIMINE LIGANDS

A THESIS

SUBMITTED IN PARTIAL FULFILLMENT OF THE REQUIREMENTS

FOR THE DEGREE OF MASTER OF SCIENCE

IN THE GRADUATE SCHOOL OF THE

TEXAS WOMAN'S UNIVERSITY

DEPARTMENT OF CHEMISTRY AND BIOCHEMISTRY

COLLEGE OF ARTS AND SCIENCES

BY

RUAA ALMOTAWA B.A.

DENTON, TEXAS

AUGUST 2014

ACKNOWLEDGMENTS

First, praise be to Allah (God), The Lord of the worlds for providing me the blessings to complete this work. Then, deepest admiration and thanks to my advisor Dr. Manal Rawashdeh-Omary for her encouragements, advice and guidance; I would not have been able to complete my thesis without her help, insight, patience and wisdom. I would like to thank my committee chair Dr. Richard Sheardy for his assistance. I am, also, grateful to my advisory committee members Dr. Mark Britt and Dr. Nasrin Mirsaleh Kohan. I would like to thank my great research group members "the Omary group members"; Daniel Korir, Waheda Hassen, Samar Kolailat, Ghada Aljomeh, Jehan Kohistani, Salimah Shamshi, Laura Hebbeln, Lorena Delgado, Mashaer Sunbul, and Erica Humbach for their help and support. My sincere gratitude, also, goes to Dr. Mohammad Omary from UNT for allowing me to use his lab. I want to express my special thanks to Dr. Vladimir Nesterov at UNT for his assistance. Their support, comments, and suggestions added valuable direction for my research. Finally, I would like to thank my lovely family; my mother, Aisha Almarzouqi, my father, Mohammed Almotawa, my husband, Abdullah Buhaimed, and my sweet daughter, Joanna for their understanding & endless love, through the duration of my studies.

ABSTRACT

RUAA ALMOTAWA

SYNTHESIS AND CHARACTERIZATION OF VARIOUS COINAGE METAL COMPLEXES WITH BRIDGING DIIMINE LIGANDS

AUGUST 2014

This thesis is a study of coinage metal complexes with various bridging diimine ligands. It has 75pp, 4 tables, 55 figures and the references for the study of group 11 elements. It discusses one main project divided by three chapters describing in general the synthesis; structure and spectroscopic studies of Silver (I) and copper (I) complexes. Chapter I discusses the introduction to trinuclear pyrazolate complexes of d^{10} coinage metals, linearly-bridging diimines, mixed-metal and mixed-ligand complexes and the potential applications, including sensors for (VOCs), metal-organic frameworks (MOFs), solar cells and organic light emitting diodes (OLEDs). Chapter II involves synthesis and characterization including x-ray crystallography, photoluminescence, 1HNMR, FT-IR, absorption spectroscopy and thermogravimetric analysis, of silver complexes, copper complexes, mixed-metal complexes and mixed-ligand complexes. Chapter III summarizes the conclusion of the results obtained in Chapter II and the expected applications.

TABLE OF CONTENTS

LIST OF TABLES

Table Page

LIST OF FIGURES

Figure Page

CHAPTER I

THE INTRODUCTION OF THE CHEMISTRY OF COINAGE METAL COMPLEXES

This thesis covers a study of synthesis, characterization and spectroscopy of d^{10} coinage metal complexes. Section 1.1 describes the introduction to trinuclear pyrazolate complexes of d^{10} coinage metals. Section 1.2 describes the introduction to linearly-bridging diimine. Section 1.3 briefly describes the mixed-metal complexes and mixed ligand complexes. In section 1.4, we discuss the potential applications for coinage metal-ligand complexes.

1.1 Trinuclear pyrazolate complexes of d^{10} coinage metals

A number of luminescent materials including d^{10} coinage metal complexes have been a subject of interest in the past few years due to the metal-metal and metal-ligand bonding natures that create unique properties [1, 2]. One of the most prominent aspects of d^{10} coinage metal chemistry is the interesting photophysical and photochemical properties for its complexes [3]. The fundamental luminescent properties of such complexes appeared from the lowest lying triplet excited states influenced by both ligand-centered π-π* and metal-to-ligand charge transfer (MLCT) transitions [4]. Trinuclear pyrazolate complexes of d^{10} coinage metals, such as Cu (I), Ag (I), and Au (I) represent a significant group of compounds that offer interesting structural architectures and intriguing properties. They often show various degrees of intermetallic M…M bonds that lead to supramolecular assemblies. By looking carefully to such complexes, trinuclear d^{10} complexes provide strong and long-living luminescence [1, 2] at ambient and cryogenic temperatures in the solid

state with tunable emissions spanning through the visible region [1, 2]. An attractive chemistry appears through the coordination between nitrogen, which is considered a “hard” element and among the “soft” metal ions, [5] including group 11 elements to introduce pyrazolates, carbeniates, and benzylimidazolates, and other linked ligands [6-8].Fackler and co-workers introduced trinuclear pyrazolate complexes of group 11 elements [9]. Pyrazole provides rich coordination chemistry [10] and exhibits exo-bidentate behavior beside the monodentate and endo-bidentate behaviors. Molecular triangles are some of the most significant molecules that have been well studied among the supramolecular complexes [11]. The pyrazolate ligands behave as the angular building blocks with well-defined turning angles, while the linear units are represented by two-coordinated metal ions (e.g. M = Ag+, Au+) [11].

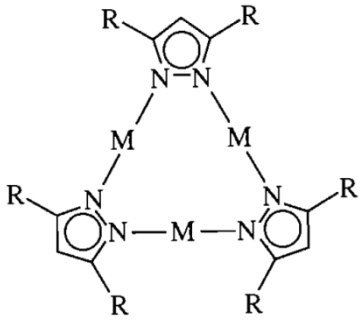

Fig. 1 exhibits planar nine-membered M3N6 rings. M= Au, Ag, Cu. R= CH_3 [14].

The R substituents (Fig. 1) at the pyrazolate ligand are major factors that can determine π-Lewis acid-base chemistry. When R groups are electron rich such as hydrogen or methyl, the overall structure shows up as a π-Lewis base [12, 13]. However, when the R groups are electron poor such as fluorinated groups, the overall structure shows up as a π-Lewis acid [12, 13]. Methylated copper (I) pyrazolate complex, {[3, 5-$(CH_3)_2$Pz]Cu}$_3$, was first reported in 1989 (Fig 1) [14], showing weak intertrimer interactions due to the Cu-Cu distance (of 2.946 Å) that is close to the sum of van der Waals radii (2.86 Å) (Fig. 2) [14]. On the other side, Dias and co-workers first introduced trinuclear complexes of Cu(I) and Ag(I) with fluorinated pyrazolates [3,5-$(CF_3)_2$Pz] (Fig. 3) [13].

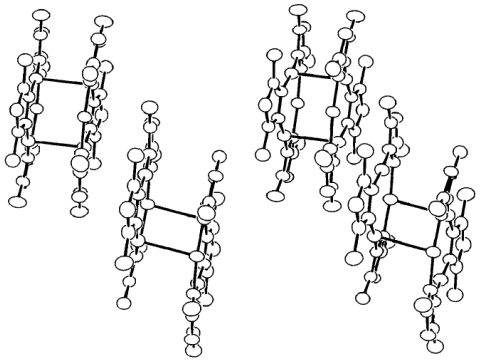

Fig. 2 exhibits stereoscopic view tris[(3,5-dimethylpyrazolat)$_2$ Cu]$_3$, showing the trimer-trimer Cu….Cu interactions [14].

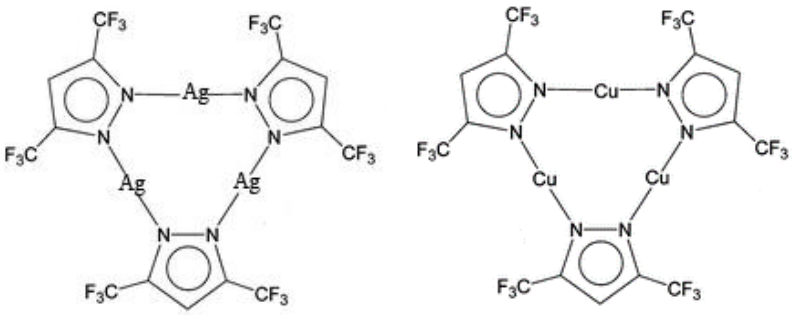

Fig. 3 Structural diagram of the trinuclear silver (I) and copper (I) pyrazolate complexes $\{[3,5\text{-}(CF_3)_2Pz]Cu\}_3$,$\{[3,5\text{-}(CF_3)_2Pz]Ag\}_3$[13].

The overall structures, based on π- Lewis acid-base chemistry, are a π-Lewis acid because of the fluorinated groups [13]. The trinuclear complexes of fluorinated pyrazolates of gold (I), copper (I), and silver (I) [13] show stronger intertrimer interaction due to the Cu-Cu distance (of 3.242 Å) that is much longer than the sum of van der Waals's radii (2.80 Å) [13], compared to $\{[3,5\text{-}(CH_3)_2Pz]Cu\}_3$ [14]. Beyond that, it was found that there are interesting properties expanding the interest in fluorinated copper (I) and silver (I) pyrazolate complexes [15]. Fluorination to metal shows many advantages, such as improving thermal and oxidative stability and eliminating the concentration of quenching [15]. At room temperature, fluorinated silver (I) pyrazolate complex has no luminescence, while copper (I) showed bright orange luminescence upon exposure to UV radiation [12]. These trinuclear coinage metal pyrazolates also show interesting π -acid/base properties in which the acidity and basicity can be controlled by the metal atom, as well as by the substituents on the pyrazole ring, [12, 16, 17]. The presence of metallophilic interactions between closed-shell transition metal plays a successful role in enhancing luminescent

properties for many group 11 complexes [16, 18]. The unit cell dimensions and emission energies of these complexes [19] with temperature modification lead to luminescent thermochromism [19,20].

1.2 Linearly-bridging diimine ligands

Bridging ligands play a significant role in facilitating the intramolecular metallophilic interactions of monovalent d^{10} complexes [21]. Chelating amines, which act as a Lewis base, become better ligands interacting with transition metal centers. Metal ions coordinate to the lone pairs of nitrogen in pyridine ligands [13]. Pyridine-based linkers are chosen as birding ligands based on two considerations: (1) the spacers linking two diimine (dipyridyl) groups in the bridging ligand would modulate the intermetallic distances, and (2) the bridging ligand conjugation helps to form metal−metal interaction [22]. Additionally, using variation of pyridine ligands leads to the most remarkable features of modulating the lifetime of emissions and the ability of adjusting the luminescence colors [22].

The chemistry of π–Lewis acid-base reactions, supramolecular structures, metalloaromaticity, metal-metal interaction, and metallophilic bonding has been described through the coordination of coinage d^{10} metals such as gold, copper and silver with a variety of bridging ligands [23]. Different factors such as the nature of the ligand, substituent groups around the ligand, the metal center, rigidity of medium, concentration, reaction time, temperature, and solvent strongly affect the chemical and photophysical properties, including the phosphorescence, fluorescence and lifetimes of the coinage metal because of their high degrees of sensitivity [24]. Cyclic trinuclear complexes of the coinage metal

complexes can undergo interaction with pyridine or imine Lewis base moieties to form dinuclear species. In a previous investigation, collidine broke the cyclic trimer units to form 3-coordinate silver and copper dinuclear moieties (Fig. 4) [19].

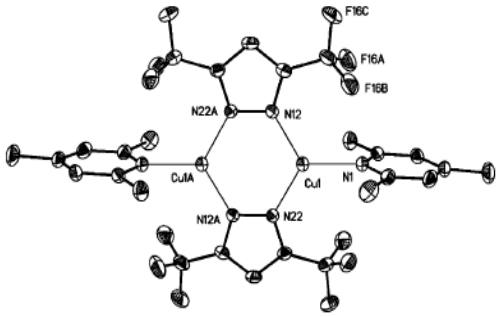

Fig. 4 A molecular structure of copper dinuclear moiety [19].

1.3 Mixed-metal complexes and mixed ligand complexes

Such studies describing metal with ligand complexes are not only applied for homometallic analogues [25-27] but also their heterometallic analogues [28]. Prior examples of heterometallic cyclic trimers include structural and luminescence studies of combining two homometallic cyclic trimers with different ligands and/or metals to tune the properties from those of the homometallic analogues [21,29]. The heterometallic cyclic trimers have been structurally identified and characterized with attractive and emissive features by combining two homometallic cyclic trimers with different ligands to form mixed metal/ligand complexes [35].

Considering the example of cyclic trinuclear silver-gold bimetallic clusters (Fig. 5) [30,31], interesting structural and bonding properties attracted the attention towards potential applications, such as medicine [32] and electronic devices [33].

Mixing ligands has been described, also, in a previous work [34]. The example of mixed-ligand tetranuclear gold (I) complexes results from a reaction of less bulky amidinates and pyrazolates with the bulky ligand dinuclear Au_2(2,6-Me_2Ph-form)$_2$ [34] (Fig. 6). The steric effect of the bulky ligands can block the formation of the tetranuclear species that allow for isolation of the dinuclear and trinuclear complexes [34].

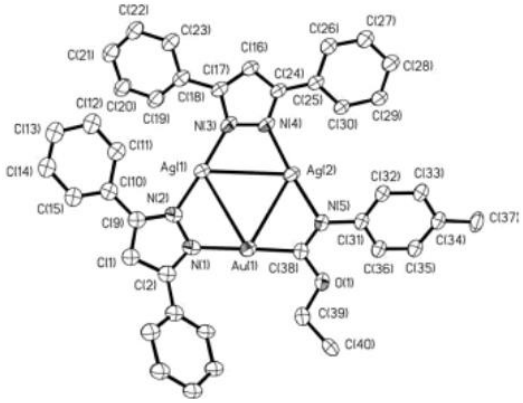

Fig. 5 A molecular structure of mixed metal gold/silver trimer [Au(carb)Ag_2(μ-3,5 Ph_2pz)$_2$] [30,31].

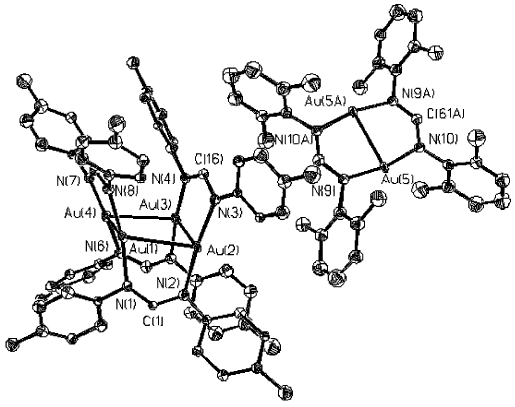

Fig. 6 A molecular structure of mixed ligands dinuclear Au_2(2,6-Me_2Ph-form)$_2$ [34].

1.4 Potential applications

The fundamental properties of d^{10} coinage metal complexes enhance their applications.

Trinuclear complexes of coinage metals present attractive π-acid/base properties upon exposure to benzene and its derivatives [35-37]. The exposure to Volatile Organic Compounds (VOC) is strongly regulated in US because they are hazardous, and others such as benzene are carcinogenic [35-37]. Accordingly, sensors for VOCs were essential to eliminating the exposure to such compounds [35-37]. Using luminescent materials as selective on/off sensors for benzene and other VOCs, such as toluene and mesitylene, was a great discovery reported by Rawashdeh-Omary et al upon using a trinuclear silver (I) pyrazolate complex [35-37].

Recently, metal-organic frameworks (MOF), also known as porous coordination polymers, have been one of the vital applications and one of the fastest growing fields in chemistry [38a]. MOFs link rigid organic ligands to metal by strong bonds [38a]. The motivation behind the prompt expansion of this field lies in the significant properties of porous MOFs compared to the known inorganic zeolites and porous carbon materials with their wide applications, such as catalysis, luminescence, magnetism, and gas storage [38 b-h]. Under what is called ‘‘reticular synthesis’’ [38 i, j], which involves tuning the length of the organic ligands, the pore sizes of porous MOFs can be changed from angstroms to nanometers [38 k]. Moreover, based on the design of the organic ligands, the pore walls of porous MOFs can be functional in particular applications [38 l-n]. These two features cannot be attained

easily in porous carbon materials and inorganic zeolites [38 b]. Additionally, porous MOFs are fascinating because of their unique surface area [38 k]. MOF-177 (Fig. 7), synthesized by Dr. Yagi et al [43], is an example of the highest surface area of 5640 m^2/g [39] among several porous MOFs. The lengthening of the linkers allows larger molecules to be presented inside the porous MOFs (Fig. 8) [40].

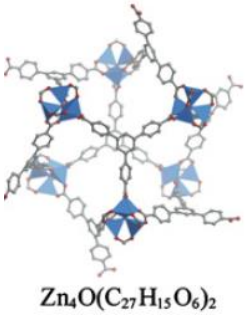

Fig. 7 A crystal structure of MOF-177 [39].

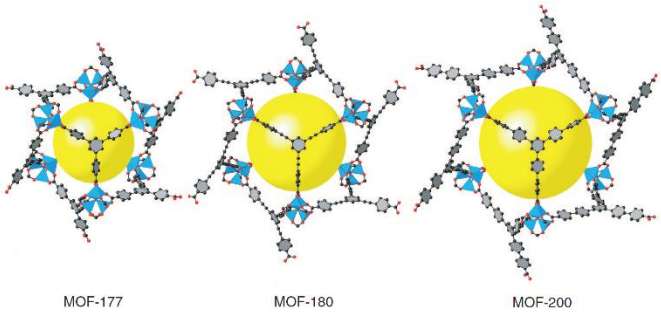

Fig. 8 Crystal structures showing the expansion from MOF-177 (left) to MOF-180 (middle) and MOF-200 (right) with associated linkers above [40].

Such compounds have a high capacity for gas storage, such as hydrogen and methane [41]. MOFs also have the potential to be used as size and shape selective catalysis, and as optoelectronic devices, etc [42].

Understanding and adjusting the topological and geometric relationships of MOFs helps to produce such structures with the coordination properties of the metal ions [42]. Porous MOFs have been ideal sources for hydrogen storage due to their structures, variable chemical functionalities, high stabilities, and large surface areas [43]. Because hydrogen can be used to create a clean alternative fuel for vehicles and other automobiles, there is a demand for the design of new materials capable of storing hydrogen at high volumetric and gravimetric densities [43]. The micro-porous metal–organic framework, hence, has been one of the most promising candidates for these materials. Additionally, porous 3D frameworks have been popular due to their application as molecular sieves, ion sensors, and catalysts [44]. A number of 3D coordination polymers have been synthesized, mainly including Cu or Ag [44].

Beside the MOFs, solar cells of nanostructures have seen attention recently because of their potential to improve charge efficiency, producing small-scale power sources, allowing innovative conversion mechanisms, and consuming low cost procedures [45]. In previous research, the nanodome devices used as solar cells were able to absorb 93% of the incident sunlight for the visible region 400-800 nm [46b]. The research states the nanodome devices has been used for the excitonic solar cells, involving dye-sensitized cells (DSC) and hybrid organic–inorganic, which have opened a broad area of inexpensive devices with large-scale solar energy [46a]. Recently, the DSC (Fig. 9) has been one of the most efficient and stable photocells [46a]. It consists of a thick nanoparticle film that introduces a large region for light-absorbing molecules on the surface [46a]. However, because nanoparticle DSCs

depend on trap-limited diffusion, their slow mechanism reduces the efficiency of devices, especially those with long wavelengths [46a].

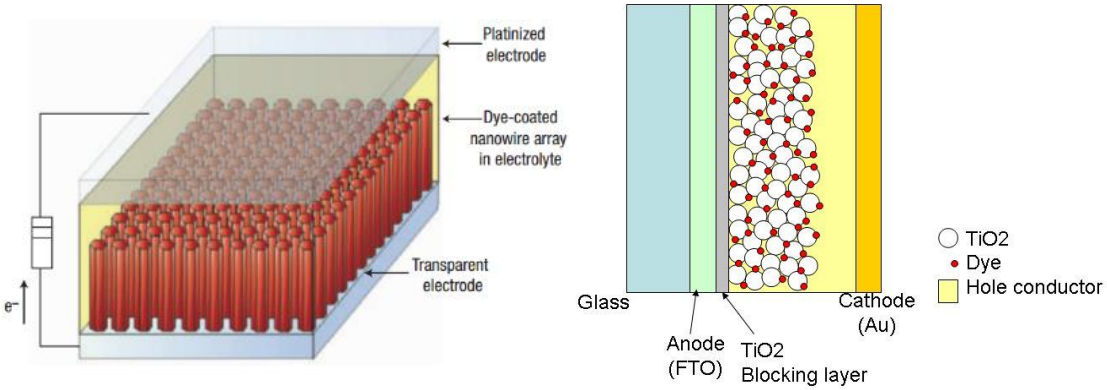

Fig. 9 A Schematic diagram of the dye-sensitized cell [21a, 50].

Both dinuclear and trinuclear complexes of monovalent coinage metals with fluorinated pyrazolate ligands exhibit interesting properties of luminescence [19]. They are emerging as promising candidates for organic light emitting diodes (OLED) that might exhibit white or monochrome electroluminescence [19]. Utilizing phosphorescent organometallic complexes in OLEDs has produced higher device performance than that with fluorescent organic materials [47]. Radiative recombination of triplet and singlet excitons has a higher limit of 100% efficiency for the phosphorescent metal-organic complexes compared to 25% for fluorescent organic materials [47]. OLEDs have been significant candidates for solid-state lighting (SSL) and display applications [47]. Such devices can significantly reduce the energy demand of a wide range of current lighting technologies, including electrical power, and video display in electronic devices such as television, cell phones, camcorders, monitors, etc [47].

A good understanding of the interaction between the metal and the ligand in the photoluminescence and absorption properties of these complexes is significant for their proposed design in order to meet the requirements for making electronic devices. In addition, studying the structure, shape and pore size of such complexes is required for particular applications.

Our research presented here might result in the formation of a coordination polymer and Metal-organic framework (MOF) due to previous work in our lab that shows a fascinating crystal structure of copper I pyrazole bipyridine (Fig. 10) [48].

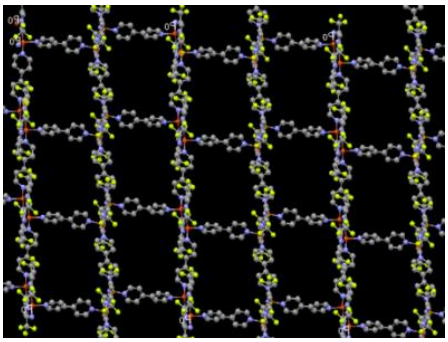

Fig. 10 3D stacking of the Copper (I) pyrazole bipyridine which shows porous properties and intermolecular interaction of Copper I [48].

This research focuses on the synthesis and characterization of new complexes of copper (I) and silver (I) with different pyridine-type imine ligands for potential applications, such as solar cells and electronic device.

CHAPTER II

THE SYNTHESIS, CHARACTERIZATION AND SPECTROSCOPY OF VARIOUS SILVER (I) AND COPPER (I) COMPLEXES

This chapter discusses the synthesis, characterization, and spectroscopy of various coinage metal complexes. The synthesis includes direct coordination of trinuclear pyrazolate complexes of silver (I) and copper (I) with the linear-bridging bipyridines. Section 2.1 covers a description of chemicals and materials used to synthesize different silver (I) and copper (I) complexes. It also describes different instruments used for the characterization. Section 2.2 considers a detailed synthetic method for silver (I) and copper (I) complexes with various linear bridgind diimine. Sections 2.3, 2.4, 2.5 and 2.5 discuss the results including the x-ray crystallographic data and the spectroscopic measurements for all silver, copper, mixed metal, and ligand complexes.

2.1 Materials and methods

All synthetic reactions were carried out under an inert atmosphere of nitrogen using standard Schlenk-line technique. 1,2-bis(4-pyridyl) ethylene (bpe), 4,4′-Trimethylenedipyridine (bpp), 1,2-bis(4-pyridyl)ethane (bpa), and piperazine (ppz), shown in figure 11, were purchased from Sigma Aldrich, and were used as received . Glassware was oven-dried at 150°C overnight. Solvents used in all experiments were purchased from Fisher ACS grade, dried in a molecular sieve, and purged using nitrogen

gas for 20 minutes before they were used. NMR solvents were purchased from Sigma Aldrich, and were used as received. NMR spectra were acquired at 25°C on Varian 400 MHz VNMRS spectrometer. The proton chemical shift is reported in ppm versus TMS. Infrared spectra were recorded on a Nicolet 6700 FT-IR spectrometer. Melting points were determined on a Mel-Tem capillary melting point apparatus. Emission and excitation spectra were recorded from PTI Spectrofluorometer equipped with a xenon lamp, a PMT detector for visible and near IR region, and an excitation correction unit. The emission spectra were corrected for detector wavelength response, while the excitation spectra were corrected for wavelength-dependent lamp intensity. Temperature-dependent emission at 77K was performed by using liquid nitrogen as a coolant. Lifetime measurements were acquired using a high speed pulsed xenon lamp source interfaced to the PTI instrument, along with an autocalibrated "Quadrascopic" monochromators for excitation wavelength selection. The absorption spectra were recorded with a Perkin-Elmer Lambda 900 double beam and a UV/VIS/NIR detector. The emission and excitation spectra have been corrected for the wavelength-dependent lamp intensity and detector response. Thermogravimetric analysis data were recorded on a TA Q50 TGA equipped with high sensitivity balance and Integrated Mass Flow Controllers. The products were weighed on the milligram scale, and burned at 700^{o}C. The weight percent of each component was analyzed and then compared with the theoretical percent. X-ray single crystal studies were performed on a CCD Bruker SMART APEX diffractometer with an Oxford Instrument low temperature attachment by Dr. Vladimir Nesterov at UNT. A suitable crystal was mounted on a glass viber using 5 min epoxy. Data were collected on a Siemens P4 diffractometer at room temperature.

Structures were solved using SHELXTL 5.1 software package provided by Bruker Analytical X-ray systems, Inc[49].

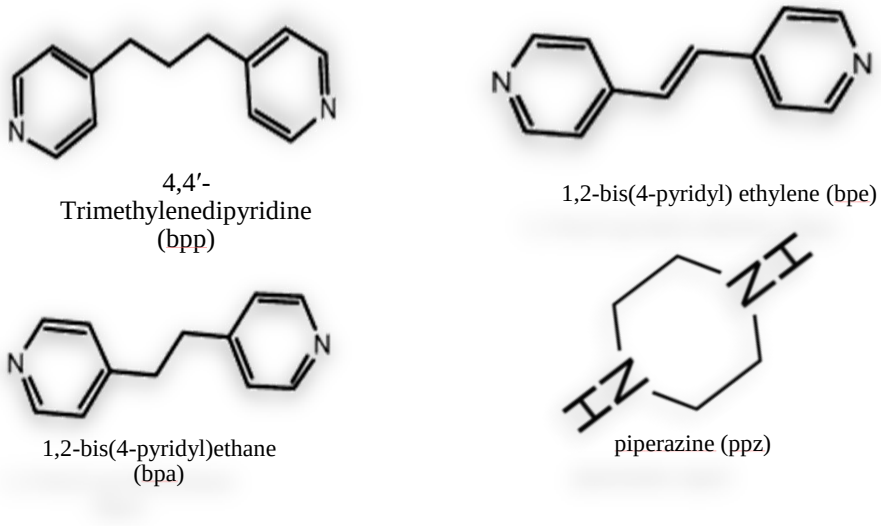

Fig. 11 A list of the ligands used as starting materials

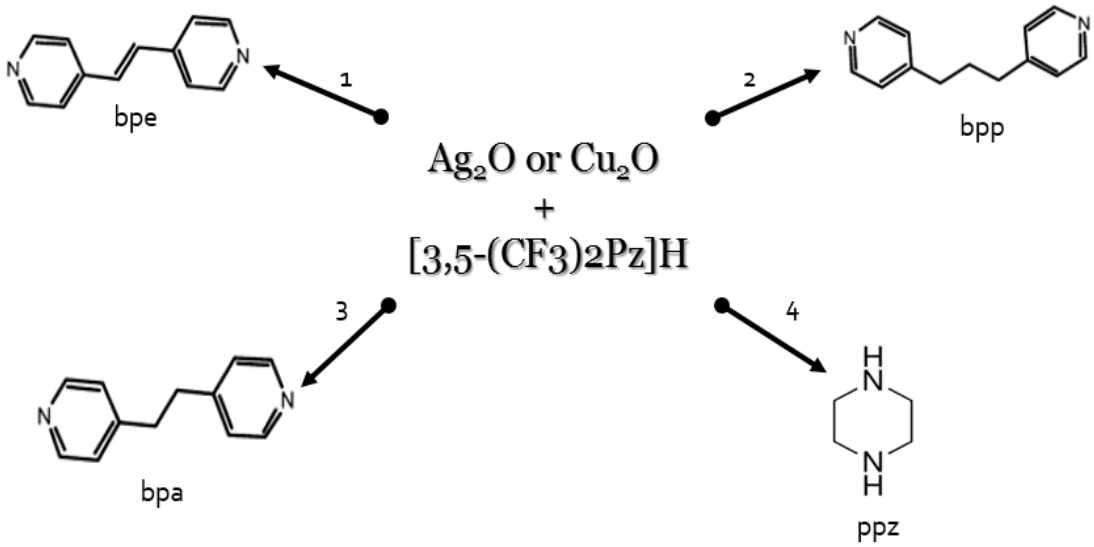

Fig. 12 The proposed synthetic route of reacting trinuclear pyrazolate complexes of silver (I) and copper (I) with the linear-bridging bipyridines

2.2 Experimental section

2.2.1. Synthesis of {[3,5-$(CF_3)_2$Pz]Ag}$_2$bpp

Ag_2O + {[3,5-$(CF_3)_2$Pz]H + bpp ⟶ {[3,5-$(CF_3)_2$Pz]Ag}$_2$bpp

Ag_2O (0.31 g, 1.35 mmol) and [3,5-$(CF_3)_2$Pz]H (0.5 g, 2.45 mmol) were mixed in about 20 ml benzene to synthesize {[3,5-$(CF_3)_2$Pz]Ag}$_3$ based on literature procedure [13]. The mixture was filtered and the filtrate was collected. {[3,5-$(CF_3)_2$Pz]Ag}$_3$ (0.1 g, 1mmol) and 4,4′-trimethylenedipyridine (bpp) (0.023 g, 1 mmol) were mixed in dichloromethane (10 ml). A white precipitate started to form instantly. The product was collected using vacuum filtration and further dried under vacuuming for 2 hours. The white product obtained (Mp230^{o}C) has a green luminescence. The product was partially soluble in organic solvents. Using sonication and filtration to get a clear solution was essential to acquire the best result for recrystallization. In this case, the crystals were grown in acetonitrile using slow evaporation for 4 days in the dark at 25°C to obtain X-ray quality crystals. Thermogravimetric analysis (TGA) of silver (% wt): 18.8%.^{1}H-NMR using as reference acetone d_6 δ: 7.3 correspond to pz (C-H), 7.3 correspond to bpp(C-H), 8.5 correspond to bpp (C-H), 2.9 correspond to bpp (C-H_2) and 1.99 correspond to bpp (C-H_2); IR : aromatic C-H stretch: 3012.33 cm^{-1}, aliphatic C-H stretch: 2855.85 cm^{-1}, C=N stretch: 2328.72 cm^{-1}, aromatic C=C bend:1613.62 cm^{-1}, aromatic C-C stretch:1519.64 cm^{-1}.It is essential to point out that the changing molar ratio of the ligand from a ratio 1:1 to ratio of 1:2 and 1:6 resulted in the same product which exhibited a green luminescence property.

Also, it is important to mention that the white product changed to yellow at 120°C and melted at 230°C.

2.2.2. Synthesis of {[3,5-$(CF_3)_2$Pz]Ag}$_2$bpe

Ag_2O + {[3,5-$(CF_3)_2$Pz]H + bpe ⟶ {[3,5-$(CF_3)_2$Pz]Ag}$_2$bpe

Ag_2O (0.31 g, 1.35 mmol) and [3,5-$(CF_3)_2$Pz]H (0.5 g, 2.45 mmol) were mixed in about 20 ml benzene to synthesize {[3,5-$(CF_3)_2$Pz]Ag}$_3$ based on literature procedure [13]. The mixture was filtered and the filtrate was collected. {[3,5-$(CF_3)_2$Pz]Ag}$_3$ (0.1 g, 1mmol) and 1,2-bis(4-pyridyl) ethylene (bpe) (0.022 g, 1 mmol) were mixed in dichloromethane (10 ml). A white precipitate started to form instantly. The product was collected using vacuum filtration and further dried under vacuuming for 2 hours. The white product obtained (Mp250^{o}C) has no luminescence. The product was partially soluble in organic solvents. Using sonication and filtration to get a clear solution was essential to acquire the best result for recrystallization. In this case, the crystals were grown in acetonitrile using slow evaporation for 4 days in the dark at 25°C to obtain X-ray quality crystals. Thermogravimetric analysis (TGA) of silver (% wt): 19.39%. ^{1}H-NMR using as reference acetone d_6 δ: 7.1 correspond to bpe (C-H), 7.40 correspond to bpe (C-H) and Pz (C-H), 8.40 correspond to bpe (C-H); IR: aromatic C-H stretch: 3150.06 cm^{-1}, aliphatic C-H stretch: 3027.47 cm^{-1}, C=N stretch: 2320.54 cm^{-1}, aromatic C=C bend:1605.45 cm^{-1}, aromatic C-C stretch:1507.38 cm^{-1}. It is essential to point out that the changing molar ratio of the ligand

from a ratio 1:1 to ratio of 1:2 and 1:6 resulted in the same product. Also, it is important to mention that the white product changed to yellow at 200°C and meltd at 250°C.

2.2.3. Synthesis of {[3,5-$(CF_3)_2$Pz]Ag}$_4$ppz

Ag_2O + {[3,5-$(CF_3)_2$Pz]H + ppz ⟶ {[3,5-$(CF_3)_2$Pz]Ag}$_4$ppz

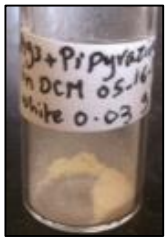

Ag_2O (0.31 g, 1.35 mmol) and [3,5-$(CF_3)_2$Pz]H (0.5 g, 2.45 mmol) were mixed in about 20 ml benzene to synthesize {[3,5-$(CF_3)_2$Pz]Ag}$_3$ based on literature procedure [13]. The mixture was filtered and the filtrate was collected. {[3,5-$(CF_3)_2$Pz]Ag}$_3$ (0.1 g, 1mmol) and piperazine (ppz) (0.132 g, 6 mmol) were mixed in dichloromethane (10 ml). The product was collected using vacuum filtration and further dried under vacuuming for 2 hours. The white product obtained (decomposed at 250ºC) has no luminescence. The product was insoluble in organic solvents, such as benzene or acetonitrile. Using sonication and filtration was essential to acquire the best result for recrystallization. In this case, the crystals were grown in acetonitrile using slow evaporation for 4 days in the dark at 25°C to obtain X-ray quality crystals. Thermogravimetric analysis (TGA) of silver (% wt): 41.82%. ^{1}H-NMR using as reference acetone d_6 δ: 7.1 correspond to pz (C-H), 2.85 correspond to ppz (C-H_2), 1.90 correspond to ppz (N-H); IR: N-H stretch: 3276.73 cm^{-1}, aromatic C-H stretch: 3020.98 cm^{-1}, aliphatic C-H stretch: 2847.67 cm^{-1}, C=N stretch: 2353.23 cm^{-1}, aromatic C=C bend:1531.90 cm^{-1}, aromatic C-C stretch:1433.83 cm^{-1}.

2.2.4. Synthesis of {[3,5-$(CF_3)_2$Pz]Cu}$_n$ bpe$_n$

Cu_2O + {[3,5-$(CF_3)_2$Pz]H + bpe ⟶ {[3,5-$(CF_3)_2$Pz]Cu}$_n$ bpe$_n$

1:1 ratio {[3,5-$(CF_3)_2$Pz]Cu}$_n$ bpe$_n$
1:2 ratio {[3,5-$(CF_3)_2$Pz]Cu}$_n$ bpe$_n$
1:6 ratio {[3,5-$(CF_3)_2$Pz]Cu}$_n$ bpe$_n$

Cu_2O (0.19 g, 1.43 mmol) and [3,5-$(CF_3)_2$Pz]H (0.50 g, 2.45 mmol) were mixed in 20ml of benzene to synthesize {[3,5-$(CF_3)_2$Pz]Cu}$_3$ based on literature procedure [13]. The mixture was filtered and the filtrate was collected. {[3,5-$(CF_3)_2$Pz]Cu}$_3$ (0.1 g, 1mmol) and 1,2-bis(4-pyridyl) ethylene (bpe) (0.025 g, 1 mmol) were mixed in benzene (10 ml). A yellow precipitate started to form instantly. The product was collected using vacuum filtration and further dried under vacuuming for 2 hours. The yellow product obtained (Mp100^{o}C) has no luminescence. The product was very soluble in acetone and acetonitrile. Several attempts of crystallization were unsuccessful in producing X-ray quality crystals because of its high sensitivity to air. Thermogravimetric analysis (TGA) of copper (% wt): 9.0%. ^{1}H-NMR using as reference acetone d_6 δ: 7.21 correspond to pz (C-H), 7.42 correspond to bpe (C-H), 8.51 correspond to bpe (C-H); IR: aromatic C-H stretch: 3035.64 cm^{-1}, aliphatic C-H stretch: 2647 cm^{-1}, C=N stretch: 2320.54 cm^{-1}, aromatic C=C bend: 1805.68 cm^{-1}, aromatic C-C stretch: 1601.36 cm^{-1}. It is essential to point out that the changing molar ratio of the ligand from a ratio 1:1 to ratio of 1:2 and 1:6 resulted in different products which have orange color for 1:2 and red color for 1:6. The melting point also changed to 125^{o}C for 1:2 and 153^{o}C for 1:6. ^{1}H-NMR using as reference CD2Cl_2 showed similar results for all different ratios.

2.2.5. Synthesis of {[3,5-$(CF_3)_2$Pz]Cu}$_n$ ppz$_n$

Cu_2O + {[3,5-$(CF_3)_2$Pz]H + ppz ⟶ {[3,5-$(CF_3)_2$Pz]Cu}$_n$ ppz$_n$

Cu_2O (0.19 g, 1.43 mmol) and [3,5-$(CF_3)_2$Pz]H (0.50 g, 2.45 mmol) were mixed in 20ml of benzene to synthesize {[3,5-$(CF_3)_2$Pz]Cu}$_3$ based on literature procedure [13]. The mixture was filtered and the filtrate was collected. {[3,5-$(CF_3)_2$Pz]Cu}$_3$ (0.1 g, 1 mmol) and piperazine (ppz) (0.034 g, 6 mmol) were mixed in benzene (10 ml). A green precipitate started to form instantly. The product was collected using vacuum filtration and further dried under vacuuming for 2 hours. The green product obtained (Mp105^{o}C) has no luminescence. The product was very soluble in acetone and acetonitrile. Several attempts of crystallization were unsuccessful in producing suitable crystals because of its high sensitivity to air. Thermogravimetric analysis (TGA) of copper (% wt): 7.9%. ^{1}H-NMR using as reference acetone d_6 δ: 7.4 correspond to pz (C-H), 2.1 correspond to ppz (C-H); IR: N-H stretch: 3293.08 cm^{-1}, aromatic C-H stretch: 3008.78 cm^{-1}, aliphatic C-H stretch: 2851.76 cm^{-1}, C=N stretch: 2324.63 cm^{-1}, aromatic C=C bend: 1670.83 cm^{-1}, aromatic C-C stretch: 1523.72 cm^{-1}.

2.2.6. Synthesis of {[3,5-$(CF_3)_2$Pz]AgCu}$_2$bpa$_2$

Cu_2O + {[3,5-$(CF_3)_2$Pz]H

+ bpa ⟶ {[3,5-$(CF_3)_2$Pz]AgCu}$_2$ bpa$_2$

Ag_2O + {[3,5-$(CF_3)_2$Pz]H

Cu_2O (0.19 g, 1.43 mmol) and [3,5-$(CF_3)_2$Pz]H (0.50 g, 2.45 mmol) were mixed in 20ml of benzene to synthesize {[3,5-$(CF_3)_2$Pz]Cu}$_3$ based on literature procedure [13]. The mixture was filtered and the filtrate was collected. Ag_2O (0.31 g, 1.35 mmol) and [3,5-$(CF_3)_2$Pz]H (0.5 g, 2.45 mmol) were mixed in about 20 ml benzene to synthesize {[3,5-$(CF_3)_2$Pz]Ag}$_3$ based on literature procedure [13]. The mixture was filtered and the filtrate was collected. {[3,5-$(CF_3)_2$Pz]Cu}$_3$ (0.048 g, ½ mmol), {[3,5-$(CF_3)_2$Pz]Ag}$_3$ (0.05 g, ½ mmol), and 1,2-bis(4-pyridyl)ethane (bpa), (0.055 g, 6 mmol) were mixed in benzene (10 ml). A light yellow precipitate started to form instantly. The product was collected using vacuum filtration and further dried under vacuuming for 2 hours. The light yellow product obtained (Mp145^{o}C) has yellow-green luminescence. The product was insoluble in organic solvents, such as benzene or acetonitrile. Using sonication and filtration was essential to acquire the best result for recrystallization. In this case, the crystals were grown in dichloromethane using slow evaporation for 2 days under nitrogen atmosphere at 25°C to obtain X-ray quality crystals. Thermogravimetric analysis (TGA) of copper and silver (% wt): 11.86%. ^{1}H-NMR using as reference acetonitrile $d_3\delta$: 7.40 correspond to pz (C-H), 7.24 correspond to bpa (C-H), 8.56 correspond to bpa (C-H), 2.92 correspond to bpa (C-H_2); IR: aromatic C-H stretch: 3064.25 cm^{-1}, aliphatic C-H stretch: 2953.92 cm^{-1}, C=N stretch: 2349.15 cm^{-1}, aromatic C=C bend:1605.45 cm^{-1}, aromatic C-C stretch:1519.64 cm^{-1}.

2.2.7. *Synthesis* $\{[3,5\text{-}(CF_3)_2Pz]AgCu\}_n\,bpe_n$

$$Cu_2O + \{[3,5\text{-}(CF_3)_2Pz]H$$
$$+ bpe \longrightarrow \{[3,5\text{-}(CF_3)_2Pz]AgCu\}_n\,bpe_n$$
$$Ag_2O + \{[3,5\text{-}(CF_3)_2Pz]H$$

Cu_2O (0.19 g, 1.43 mmol) and $[3,5\text{-}(CF_3)_2Pz]H$ (0.50 g, 2.45 mmol) were mixed in 20ml of benzene to synthesize $\{[3,5\text{-}(CF_3)_2Pz]Cu\}_3$ based on literature procedure [13]. The mixture was filtered and the filtrate was collected. Ag_2O (0.31 g, 1.35 mmol) and $[3,5\text{-}(CF_3)_2Pz]H$ (0.5 g, 2.45 mmol) were mixed in about 20 ml benzene to synthesize $\{[3,5\text{-}(CF_3)_2Pz]Ag\}_3$ based on literature procedure [13]. The mixture was filtered and the filtrate was collected. $\{[3,5\text{-}(CF_3)_2Pz]Cu\}_3$ (0.048 g, ½ mmol), $\{[3,5\text{-}(CF_3)_2Pz]Ag\}_3$ (0.05 g, ½ mmol), and 1,2-bis(4-pyridyl) ethylene (bpe), (0.055 g, 6 mmol) were mixed in benzene (10 ml). An orange precipitate started to form gradually. The product was obtained by vacuum filtration and further dried by vacuuming for 2 hours. The orange product obtained (Mp190^oC) has no luminescence. The product was very soluble in acetone and acetonitrile. Although we could crystellize the product, there is a problem in producing X-ray quality crystals and collecting the X-ray data because of its high sensitivity. Thermogravimetric analysis (TGA) of copper and silver (% wt): 9.2%. ^{1}H-NMR using as reference acetone $d_6\delta$: 7.4 correspond to pz (C-H), 7.02 correspond to bpe (C-H), 7.6 correspond to bpe (C-H); IR: aromatic C-H stretch: 3150.06 cm^{-1}, aliphatic C-H stretch: 2989.47 cm-1, C=N stretch: 2324.64 cm^{-1}, aromatic C=C bend:1605.45 cm^{-1}, aromatic C-C stretch:1511.46 cm^{-1}.

2.2.8. Synthesis of {[3,5-$(CF_3)_2$Pz]AgCu}$_n$ ppz$_n$

Cu_2O + {[3,5-$(CF_3)_2$Pz]H
+ ppz ⟶ {[3,5-$(CF_3)_2$Pz]AgCu}$_n$ ppz$_n$
Ag_2O + {[3,5-$(CF_3)_2$Pz]H

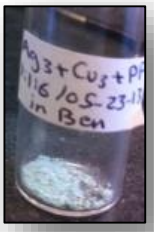

Cu_2O (0.19 g, 1.43 mmol) and [3,5-$(CF_3)_2$Pz]H (0.50 g, 2.45 mmol) were mixed in 20ml of benzene to synthesize {[3,5-$(CF_3)_2$Pz]Cu}$_3$ based on literature procedure [13]. The mixture was filtered and the filtrate was collected. Ag_2O (0.31 g, 1.35 mmol) and [3,5-$(CF_3)_2$Pz]H (0.5 g, 2.45 mmol) were mixed in about 20 ml benzene to synthesize {[3,5-$(CF_3)_2$Pz]Ag}$_3$ based on literature procedure [13]. The mixture was filtered and the filtrate was collected. {[3,5-$(CF_3)_2$Pz]Cu}$_3$ (0.048 g, ½ mmol), {[3,5-$(CF_3)_2$Pz]Ag}$_3$ (0.05 g, ½ mmol), and piperazine (ppz) (0.025 g, 6 mmol) were mixed in benzene (10 ml). A green precipitate started to form gradually. The product was collected using vacuum filtration and further dried under vacuuming for 2 hours. The orange product obtained (Mp105^{o}C) has no luminescence. The product was very soluble in acetone and acetonitrile. Several attempts of crystallization were unsuccessful in producing suitable crystals because of its high sensitivity to air. Thermogravimetric analysis (TGA) of copper and silver (% wt): 19.8%.^{1}H-NMR using as reference acetone d_6 δ: 7.41 correspond to pz (C-H), 2.22 correspond to ppz (C-H); IR: N-H stretch: 3293.08 cm^{-1}, aromatic C-H stretch: 3010.02 cm^{-1}, aliphatic C-H stretch: 2847.67 cm^{-1}, C=N stretch: 2349.15 cm^{-1}, aromatic C=C bend: 1609.53 cm^{-1}, aromatic C-C stretch:1515.55 cm^{-1}.

2.2.9. Synthesis of {[3,5-$(CF_3)_2$Pz]Ag}$_2$bpp / bpe

Ag_2O + {[3,5-$(CF_3)_2$Pz]H + bpp +bpe ⟶ {[3,5-$(CF_3)_2$Pz]Ag}$_2$bpp

Ag_2O (0.31 g, 1.35 mmol) and [3,5-$(CF_3)_2$Pz]H (0.5 g, 2.45 mmol) were mixed in about 20 ml benzene to synthesize {[3,5-$(CF_3)_2$Pz]Ag}$_3$ based on literature procedure [13]. The mixture was filtered and the filtrate was collected. {[3,5-$(CF_3)_2$Pz]Ag}$_3$ (0.1 g, 1mmol), 4,4′-trimethylenedipyridine (bpp)(0.023 g, 1 mmol) and 1,2 (4-dipyridyl ethylene) (bpe) (0.02 g, 1 mmol) were mixed in dichloromethane (10 ml). A white precipitate started to form instantly. The product was obtained by vacuum filtration and further dried by vacuuming for 2 hours. The white product obtained (Mp235^{o}C) has a green luminescence. The product was partially soluble in organic solvents. Using sonication and filtration to get a clear solution was essential to acquire the best result for recrystallization. In this case, the crystals were grown in acetonitrile using slow evaporation for 4 days in the dark at 25°C to obtain X-ray quality crystals.

2.3 Results and Discussion for Silver Complexes

Silver complexes: {[3,5-$(CF_3)_2$Pz]Ag}$_2$bpe, {[3,5-$(CF_3)_2$Pz]Ag}$_2$bpp, and {[3,5-{$(CF_3)_2$Pz]Ag}$_4$ppz were prepared by treatment of trinuclear silver (I) complex with a slight molar excess of the corresponding linear bridging diimine in dichloromethane. They were obtained in high yields (>80%). Silver complexes are air stable crystalline solids. They are partially soluble in organic solvents such as dichloromethane, acetonitrile, acetone and tetrahydrofuran but completely soluble with sonication and filtration. All these

silver complexes were characterized using ^{1}HNMR spectroscopy, FT-IR spectroscopy, absorption spectroscopy and TGA. {[3,5-$(CF_3)_2$Pz]Ag}$_2$bpp is the only one from the silver complexes which has luminescence. In this section we will discuss the photoluminescence spectra of {[3,5-$(CF_3)_2$Pz]Ag}$_2$bpp, ^{1}HNMR spectra, FT-IR and absorption properties of all silver metal complexes.

2.3.1. *{[3,5-$(CF_3)_2$Pz]Ag}$_2$bpp*

2.3.1.1. The X-ray crystallographic data

In this section, we will discuss in details the x-ray crystallographic data. Table 1(A) shows that {[3,5-$(CF_3)_2$Pz]Ag}$_2$bpp was crystallized in the $\bar{P}4$ 21c space group with tetragonal system with a = 14.5864 (9) Å, b = 14.5864 (9) Å, c = 12.8924 (8) Å, α= 90°, β = 90°, and γ = 90°. Figure 13(A) shows that {[3,5-$(CF_3)_2$Pz]Ag}$_2$bpp adopts a U shape. It shows also that silver (I) coordinates to two nitrogen from different pyrazolate ligands and one nitrogen from the pyridyl group in 4,4′-trimethylenedipyridine (bpp) ligand to form a dimer with three coordinates. The backing structures in figures 13(B,C, and D) reveal on extended chains with small porosity. All the non-hydrogen atoms were refined anisotropically. The hydrogen atoms were placed at calculated positions and refined using a riding model. The final full-matrix least-squares refinement on $F2$ gave R1:2.81% and wR2:5.41% for all data. The goodness-of-fit was 1.030. Table 1(B) shows selected bond distances (Å) and angles (°) for {[3,5-$(CF_3)_2$Pz]Ag}$_2$bpp.

Table 1

(A) X-ray Crystallographic Data for {[3,5-$(CF_3)_2$Pz]Ag}$_2$bpp, (B) Selected bond distances (Å) and angles (°) for {[3,5-$(CF_3)_2$Pz]Ag}$_2$bpp

Empirical Formula	**C23 H15 AG2 F12 N6**
Formula Weight	819.15
Temperature	200(2) K
Wavelength	0.71073 Å
Crystal System	Tetragonal
Space Group	P -4 21 C
Unit Cell Dimensions	A = 14.5864(9) Å α= 90°. B = 14.5864(9) Å β= 90°. C = 12.8924(8) Å γ = 90°.
Volume	2743.0(3) $Å^3$
Z	4
Density (Calculated)	1.984 Mg/M^3
Absorption Coefficient	1.535 Mm^{-1}
F(000)	1588
Crystal Size	0.29 X 0.22 X 0.11 Mm^3
Theta Range For Data Collection	1.97 To 27.10°
Index Ranges	-18<=H<=18, -18<=K<=18, -16<=L<=16
Reflections Collected	32539
Independent Reflections	3031 [R(Int) = 0.0323]
Completeness To Theta =2 7.12°	100.0%
Absorption Correction	Semi-Empirical From Equivalents
Max. And Min. Transmission	0.8493 And 0.6670
Refinement Method	Full-Matrix Least-Squares On F^2
Data / Restraints / Parameters	3031 / 7 / 253
Goodness-Of-Fit On F^2	1.030
Final R Indices [I>2sigma(I)]	R1 = 0.0197, Wr2 = 0.0525
R Indices (All Data)	R1 = 0.0212, Wr2 = 0.0541
Largest Diff. Peak And Hole	0.281 And -0.262 $E.Å^{-3}$

(A)

BOND	Bond Lengths Å	BOND	Bond Lengths Å
Ag(1)-N(2)#1	2.190(2)	N(2)#1-Ag(1)-N(3)	139.49(7)
Ag(1)-N(3)	2.243(2)	N(2)#1-Ag(1)-N(1)	110.77(8)
Ag(1)-N(1)	2.324(2)	N(3)-Ag(1)-N(1)	103.35(8)
Ag(1)-Ag(1)#2	3.2664(4)	N(2)#1-Ag(1)-Ag(1)#2	64.44(6)
N(2)-Ag(1)#3	2.190(2)	N(3)-Ag(1)-Ag(1)#2	119.68(6)
		N(1)-Ag(1)-Ag(1)#2	114.38(6)

(B)

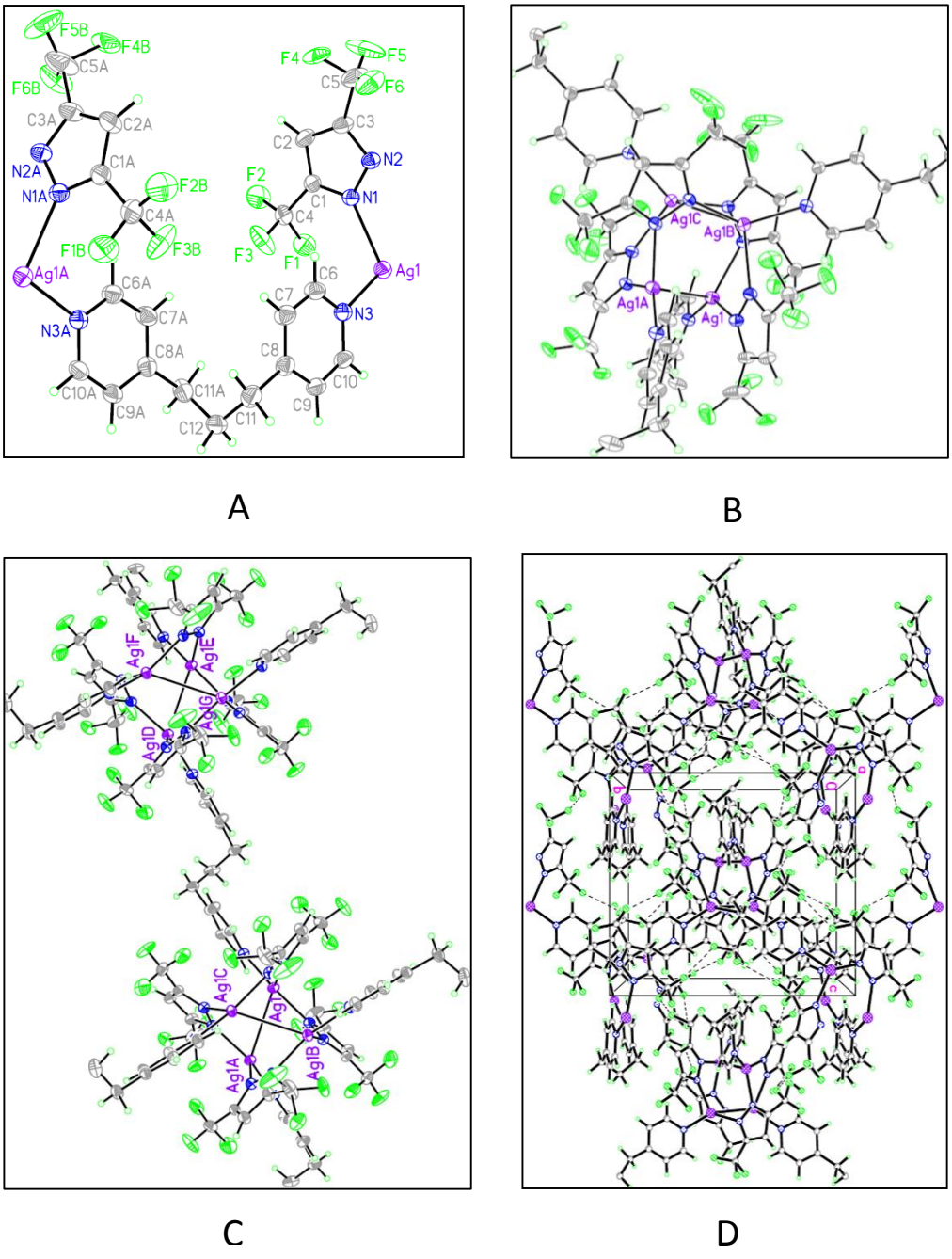

Fig. 13 Molecular structure (A) and packing (B,C and D) diagrams from the crystal structure of {[3,5-$(CF_3)_2$Pz]Ag}$_2$bpp showing extended polymeric porous phase.

2.3.1.2. Photoluminescence and absorption spectra

We will discuss with the photophysical results for {[3,5-$(CF_3)_2$Pz]Ag}$_2$bpp. The complex exhibited green photoluminescence (PL) in the solid state at room temperature (RT) and 77K. However, it didn't exhibit any PL in solution. All the steady state (emission and excitation) spectra and lifetime at RT and 77K are shown in Figures 14, 15. The photoluminescence excitation (PLE) band, with maxima at λ_{exc}= 280 nm, and the emission band, with maximum at λ_{em}= 490 nm, were observed for the solid (powder) at RT. Upon cooling to 77K, an excitation band, with maximum at 275 nm, and an emission band, with maximum at 520 nm, was observed. The RT emission lifetime is 31.69 μs, while the 77K emission lifetime is 109.3 μs, which are all suggesting phosphorescence from a triplet excited state. On the other hand, figure 16 shows intense absorption bands for {[3,5-$(CF_3)_2$Pz]Ag}$_2$bpp in the UV region due to ligand charge π-π*.

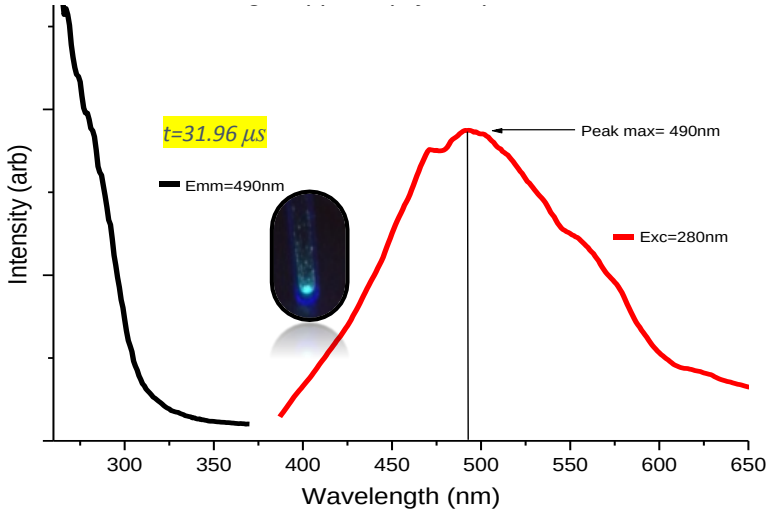

Fig. 14 Photoluminescence excitation (left) and emission (right) spectra of {[3,5-$(CF_3)_2$Pz]Ag}$_2$bpp in a solid state at RT.

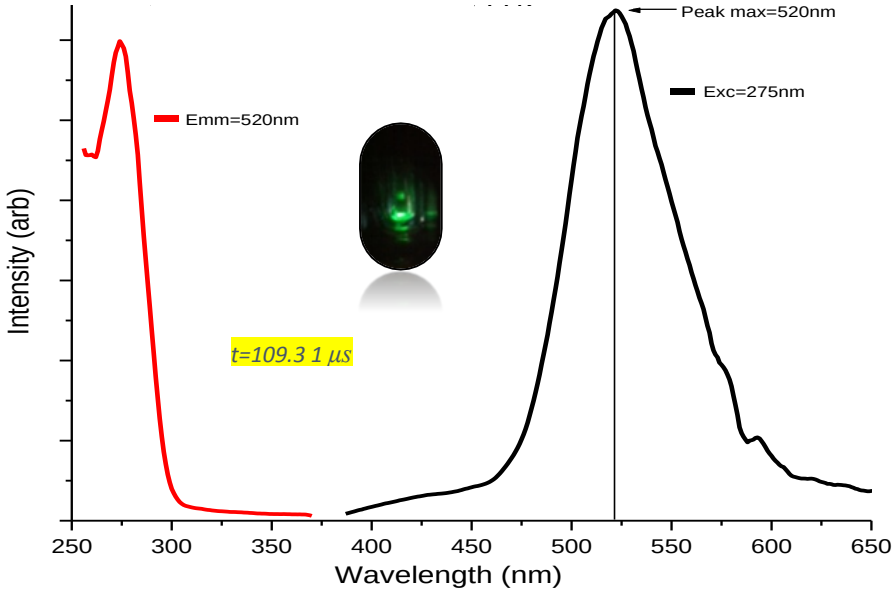

Fig. 15 Photoluminescence excitation (left) and emission (right) spectra of {[3,5-$(CF_3)_2$Pz]Ag}$_2$bpp in a solid state at 77K.

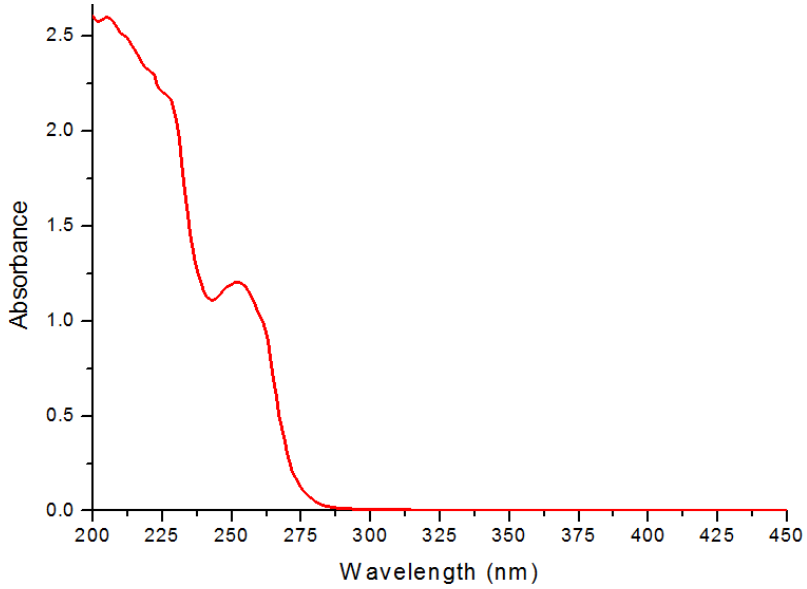

Fig. 16 The absorption spectrum of {[3,5-$(CF_3)_2$Pz]Ag}$_2$bpp in acetonitrile at RT.

2.3.1.3. Characterization using ^{1}HNMR, TGA, FT-IR spectra

^{1}H NMR measurements of {[3,5-$(CF_3)_2$Pz]Ag}$_2$bpp were done using deuterated acetone. Here we are illustrating the ^{1}H NMR spectra of {[3,5-$(CF_3)_2$Pz]Ag}$_2$bpp. As expected, the proton NMR spectra of the fluorinated silver pyrazolates lack the broad peak corresponding to the C-H proton of the pyrazoles at around δ = 7.0 [13]. However, the ^{1}H NMR signal corresponding to the protons at pyrazolyl ring 4-position shows a small downfield shift. Figure 17 represents the ^{1}H NMR spectrum of {[3,5-$(CF_3)_2$Pz]Ag}$_2$bpp. The sharp peaks at δ = 8.5, 7.3, 2.9 and 1.99 are assigned to 4,4′-trimethylenedipyridine (bpp).

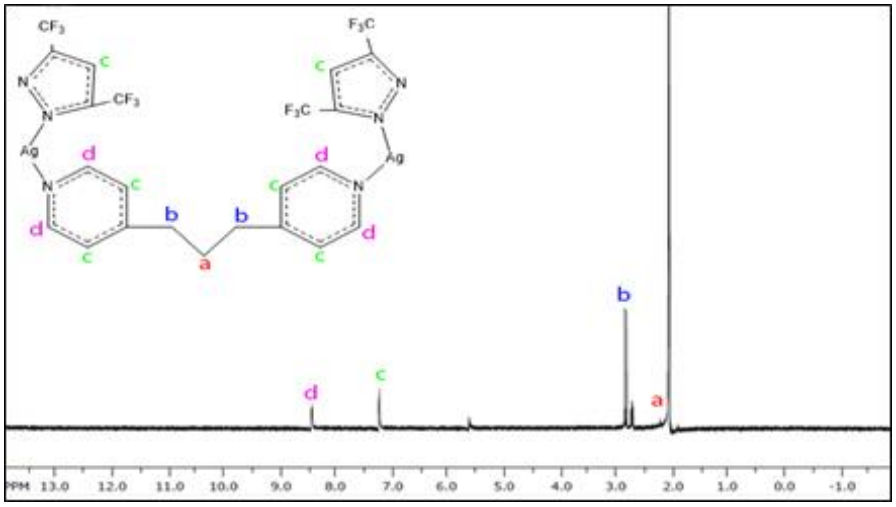

Fig. 17 ^{1}H NMR (400 MHz) spectrum of {[3,5-$(CF_3)_2$Pz]Ag}$_2$bpp in Acetone d_6

The product {[3,5-$(CF_3)_2$Pz]Ag}$_2$bpp has a formula structure: (C_{23} H_{15} Ag_2 F_{12} N_6: MW: 819.15g/mol). Ag_2 weight %= (107.86*2/819.15)x100= 26.33%. Theoretically, there is 26.33% of silver in 819.15 g/mole. TGA (Q50 V6.7) analysis in figure 18 shows that 82.21% weight loss of the organic ligands in {[3,5-$(CF_3)_2$Pz]Ag}$_2$bpp . It indicates that the

silver is left from the remaining percentage of 17.89%, which is less than the theoretical percentage. The difference between the theoretical percentage and the actual percentage is probably due to impurities and solvents in the sample (powder). The IR spectra for {[3,5-$(CF_3)_2$Pz]Ag}$_2$bpp shown in figure 19 confirms the presence of the ligands (Pz, bpp) in the product.

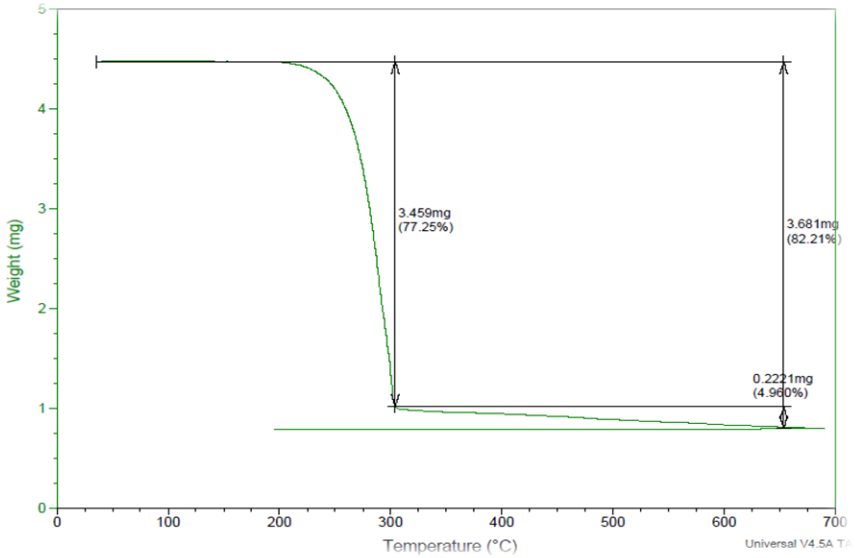

Fig. 18 TGA (Q50 V6.7) analysis of {[3,5-$(CF_3)_2$Pz]Ag}$_2$bpp

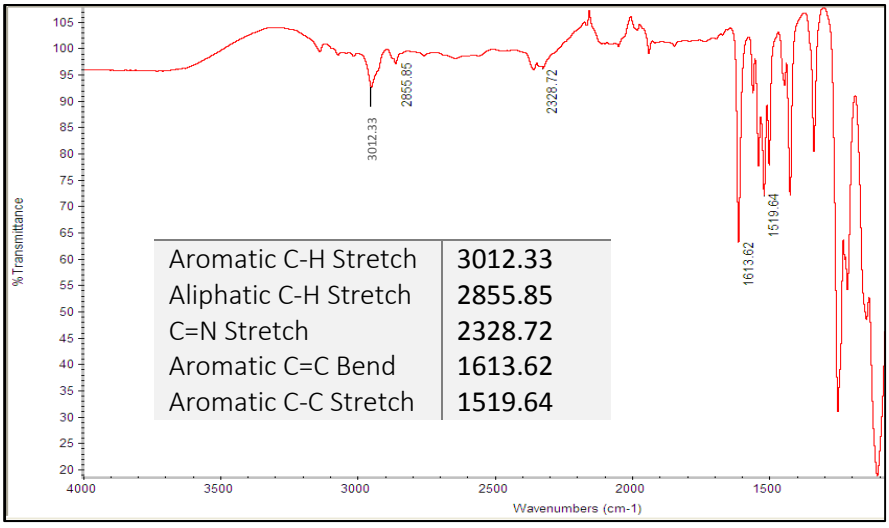

Fig. 19 FT-IR spectrum of {[3,5-$(CF_3)_2$Pz]Ag}$_2$bpp.

2.3.2. *{[3,5-$(CF_3)_2$Pz]Ag}$_2$bpe*

2.3.2.1. The X-ray crystallographic data

In this section, we will discuss in details the x-ray crystallographic data. Table 2(A) shows that {[3,5-$(CF_3)_2$Pz]Ag}$_2$bpe have the C 2/c space group with *a* = 17.4666 (18) Å, *b* = 14.5903 (15) Å, *c* = 21.961 (2) Å, α= 90°, β = 109.5350 (10)°, and γ = 90°. {[3,5-$(CF_3)_2$Pz]Ag}$_2$bpe crystallizes in monoclinic system as dimers and with one molecule in the asymmetric unit (for a Z value of 8). Figures 20(A and B) show that silver (I) coordinates with two nitrogen from pyrazolate ligand and another nitrogen from the pyridyl group in 1,2-bis(4-pyridyl) ethylene ligand to form a dimer with three coordinates. The dimers sits on an inversion center. {[3,5-$(CF_3)_2$Pz] Ag}$_2$bpe is packed in zigzag chains with small porosity as shown in figures 20(C and D). All the non-hydrogen atoms were refined anisotropically. The hydrogen atoms were placed at calculated positions and refined using a riding model. The final full-matrix least-squares refinement on *F*2 gave R1:4.93% and wR2:11.88% for all data. The goodness-of-fit was 1.070. Table 2(B) shows selected bond distances (Å) and angles (°) for {[3,5-$(CF_3)_2$Pz]Ag}$_2$bpe.

Table 2

(A) X-ray Crystallographic Data for {[3,5-$(CF_3)_2$Pz]Ag}$_2$bpe, (B) Selected bond distances (Å) and angles (°) for {[3,5-$(CF_3)_2$Pz]Ag}$_2$bpe.

Empirical Formula	**C22 H12 AG2 F12 N6**
Formula Weight	804.12
Temperature	200(2) K
Wavelength	0.71073 Å
Crystal System	Monoclinic
Space Group	C 2/c
Unit Cell Dimensions	a = 17.4666(18) Å, α= 90°. b = 14.5903(15) Å, β= 109.5350(10)°. c = 21.961(2) Å, γ = 90°.
Volume	5274.5(9) $Å^3$
Z	8
Density (Calculated)	2.025 Mg/m^3
Absorption Coefficient	1.595 mm^{-1}
F(000)	3104
Crystal Size	0.20 x 0.20 x 0.13 mm^3
Theta Range For Data Collection	1.87 to 27.05°
Index Ranges	-22<=h<=22, -18<=k<=18, -28<=l<=28
Reflections Collected	31267
Independent Reflections	5783 [R(int) = 0.0285]
Completeness To Theta =2 7.12°	99.7%
Absorption Correction	Semi-empirical from equivalents
Max. And Min. Transmission	0.8147 and 0.7357
Refinement Method	Full-matrix least-squares on F^2
Data / Restraints / Parameters	5783 / 6 / 409
Goodness-Of-Fit On F^2	1.070
Final R Indices [I>2sigma(I)]	R1 = 0.0439, wR2 = 0.1188
R Indices (All Data)	R1 = 0.0493, wR2 = 0.1248
Largest Diff. Peak And Hole	1.008 and -1.239 $e.Å^{-3}$
Extinction Coefficient	0.00084(7)

(A)

BOND	**Bond Lengths Å**	**BOND**	**Bond Lengths Å**
Ag(1)-N(3)	2.214(3)	Ag(3)-N(2)#3	2.278(3)
Ag(1)-N(5)	2.253(3)	Ag(3)-N(6)#4	2.360(3)
Ag(1)-N(1)	2.284(3)	Ag(3)-N(6)	2.360(3)
Ag(2)-N(4)	2.155(4)	N(2)-Ag(3)#2	2.278(3)
Ag(2)-N(4)#1	2.155(4)	Ag(1)-N(3)	2.214(3)
Ag(3)-N(2)#2	2.278(3)		

(B)

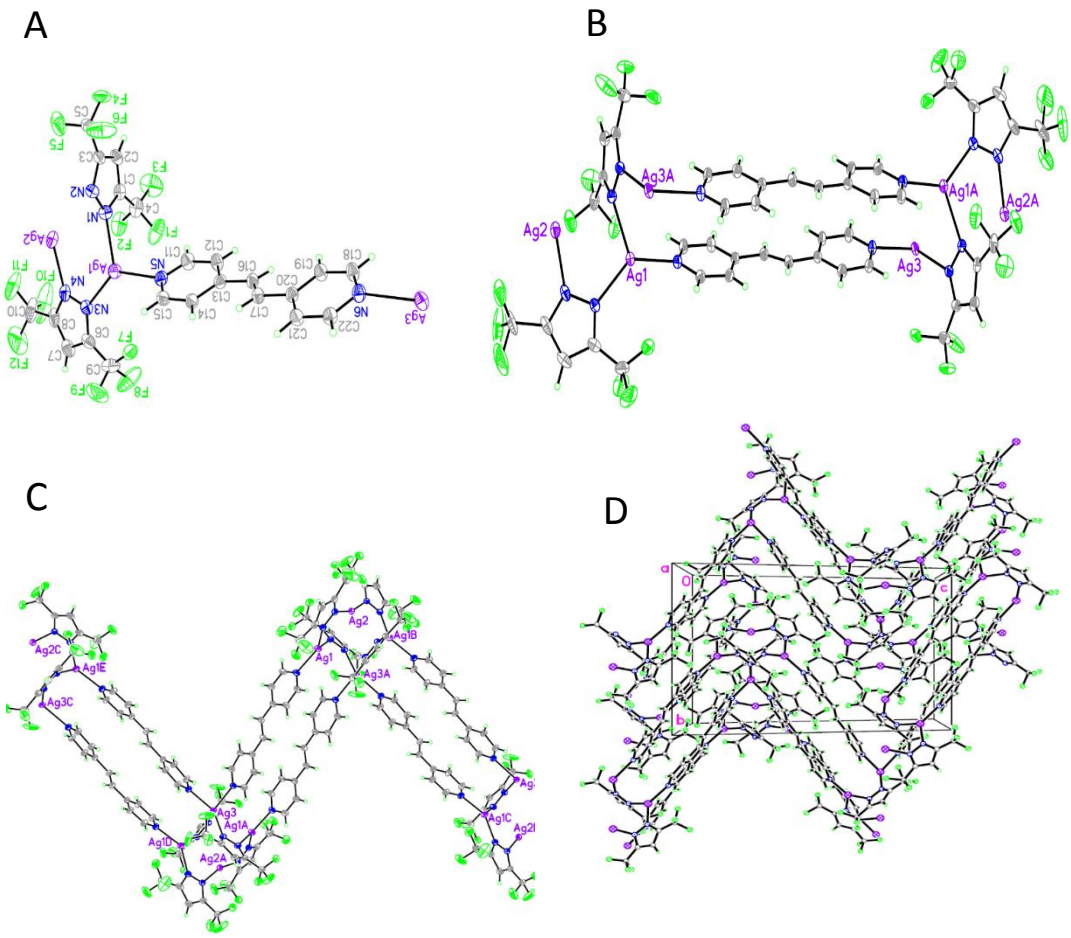

Fig. 20 Molecular structure (A) and packing (B,C and D) diagrams from the crystal structure of {[3,5-$(CF_3)_2$Pz]Ag}$_2$bpe showing extended polymeric porous phase.

2.3.2.2. Absorption spectra

Figure 21 shows intense absorption bands for {[3,5-$(CF_3)_2$Pz]Ag}$_2$bpp in the UV region due to ligand charge π-π*.

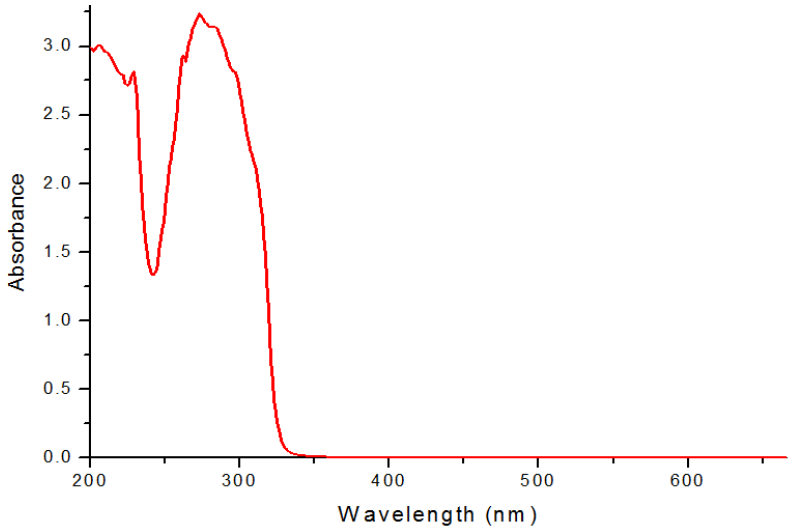

Fig. 21 The absorption spectrum of {[3,5-$(CF_3)_2$Pz]Ag}$_2$bpe in acetonitrile at RT.

2.3.2.3. Characterization using ^{1}HNMR, TGA, FT-IR spectra

^{1}H NMR measurements of {[3,5-$(CF_3)_2$Pz]Ag}$_2$bpe were done by using deuterated acetone. Here we are illustrating the ^{1}H NMR spectra of {[3,5-$(CF_3)_2$Pz]Ag}$_2$bpe. As expected, the proton NMR spectra of the fluorinated silver pyrazolates lack the broad peak corresponding to the C-H proton of the pyrazoles at around δ = 7.0 [13]. However, the ^{1}H NMR signal corresponding to the protons at pyrazolyl ring 4-position shows a small downfield shift. Figure 22 represents the ^{1}H NMR spectrum of {[3,5-$(CF_3)_2$Pz]Ag}$_2$bpe. The sharp peaks at δ =7.1, 7.40 and 8.40 are assigned to 1,2-bis(4-pyridyl) ethylene (bpe).

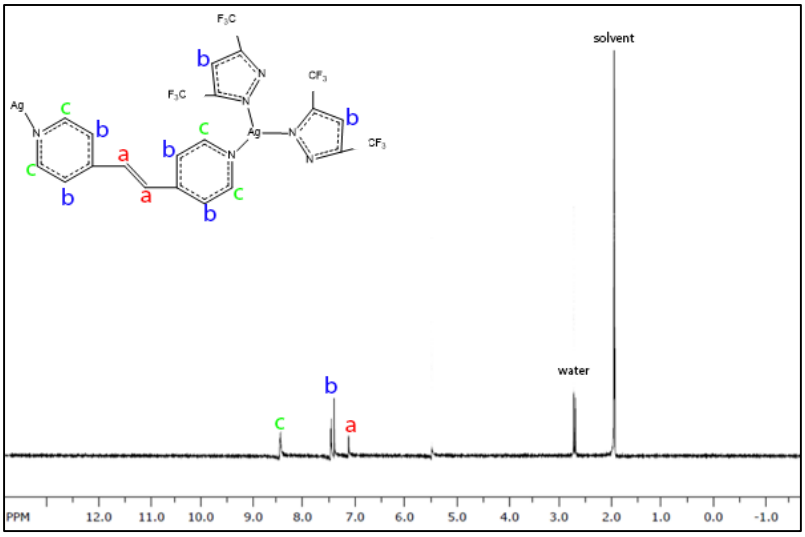

Fig. 22 ^{1}H NMR (400 MHz) spectrum of {[3,5-$(CF_3)_2$Pz]Ag}$_2$bpe in Acetone d_6.

The product {[3,5-$(CF_3)_2$Pz]Ag}$_2$bpe has a formula structure (C_{22} H_{12} Ag_2 F_{12} N_6: MW: 804.12g/mol). Ag_2 weight %= (107.86*2/804.12)x100= 26.82%. Theoretically, there is 26.82% of silver in 804.12 g/mole. TGA (Q50 V6.7) analysis in figure 23 shows that 80.71% weight loss of the organic ligands in {[3,5-$(CF_3)_2$Pz]Ag}$_2$bpe . It indicates that the silver is left from the remaining percentage of 18.39%, which is less than the theoretical percentage. The difference between the theoretical percentage and the actual percentage is probably due to impurities and solvents in the sample (powder).

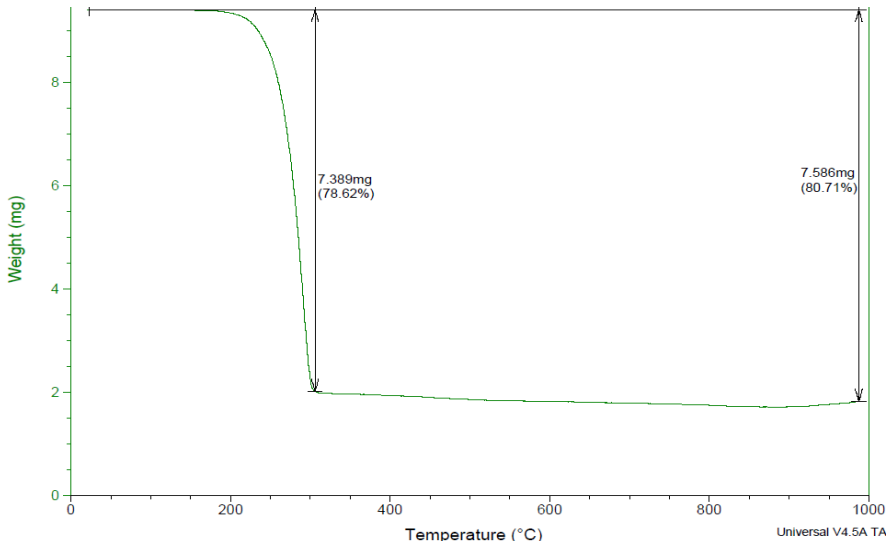

Fig. 23 TGA (Q50 V6.7) analysis of {[3,5-$(CF_3)_2$Pz]Ag}$_2$bpe

The IR spectra for {[3,5-$(CF_3)_2$Pz]Ag}$_2$bpe, shown in figure 24, confirms the presence of the ligands (Pz, bpe) in the product.

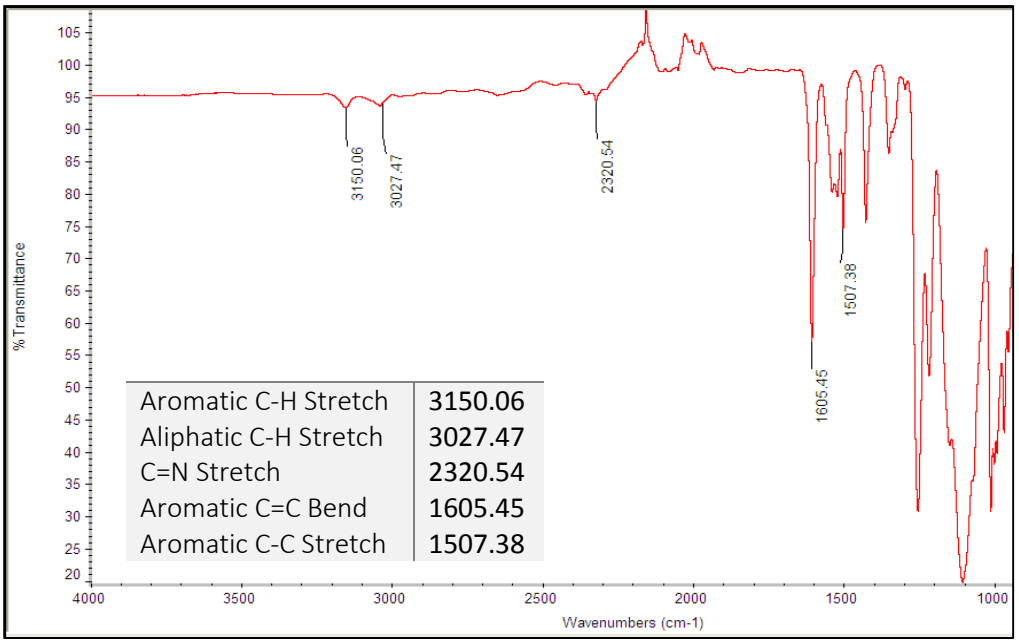

Fig. 24 FT-IR spectrum of {[3,5-$(CF_3)_2$Pz]Ag}$_2$bpe

2.3.3. *{[3,5-$(CF_3)_2$Pz]Ag}$_4$ppz*

2.3.3.1. The X-ray crystallographic data

In this section, we will discuss in details the x-ray crystallographic data. Based on table 3, the crystals obtained in {[3,5-$(CF_3)_2$Pz]Ag}$_4$ppz have C 2/c space group with a = 15.0562 (18) Å, b = 27.738 (3) Å, c = 21.0564 (14) Å, α= 90°, β = 121.855 (2)°, and γ = 90°. {[3,5-{$(CF_3)_2$Pz]Ag}$_4$ppz crystallizes in monoclinic system as dimers and with one molecule in the asymmetric unit (for a Z value of 4). Figure 25(A) shows that silver (I) coordinates to two nitrogen atoms from the pyrazole ligands and to other nitrogen from piperazine ligand to form a dimer with three coordinates. The crystal structure doesn't confirm if the nitrogen atoms of the piperazine are neutral or protonated. Otherwise, all the non-hydrogen atoms were refined anisotropically. The hydrogen atoms were placed at calculated positions, and refined using a riding model. The backing structures in figures 25(B and C) reveal on extended chains with small porosity. The final full-matrix least-squares refinement on $F2$ gave R1: 2.33% and wR2: 6.50% for all data. The goodness-of-fit was 1.043. Table 3(B) shows selected bond distances (Å) and angles (°) for {[3,5-$(CF_3)_2$Pz]Ag}$_4$ppz.

Table 3

(A) X-ray Crystallographic Data for {[3,5-$(CF_3)_2$Pz]Ag}$_4$ppz, (B) Selected bond distances (Å) and angles (°) for {[3,5-$(CF_3)_2$Pz]Ag}$_4$ppz.

Empirical Formula	**C28 H20 AG4 F24 N12**
Formula Weight	1412.04
Temperature	100(2) K
Wavelength	0.71073 Å
Crystal System	Monoclinic
Space Group	C 2/c
Unit Cell Dimensions	a = 15.0562(18) Å, α= 90°. b = 27.738(3) Å, β= 121.855(2)°. c = 12.0564(14) Å, γ = 90°.
Volume	4276.8(9) $Å^3$
Z	4
Density (Calculated)	2.193 Mg/m^3
Absorption Coefficient	1.950 mm^{-1}
F(000)	2704
Crystal Size	0.21 x 0.20 x 0.07 mm^3
Theta Range For Data Collection	1.75 to 27.09°.
Index Ranges	-19<=h<=19, -35<=k<=35, -15<=l<=15
Reflections Collected	28523
Independent Reflections	4718 [R(int) = 0.0291]
Completeness To Theta =2 7.12°	99.8 %
Absorption Correction	Semi-empirical from equivalents
Max. And Min. Transmission	0.8837 and 0.6884
Refinement Method	Full-matrix least-squares on F^2
Data / Restraints / Parameters	4718 / 0 / 307
Goodness-Of-Fit On F^2	1.043
Final R Indices [I>2sigma(I)]	R1 = 0.0215, wR2 = 0.0631
R Indices (All Data)	R1 = 0.0233, wR2 = 0.0650
Largest Diff. Peak And Hole	1.073 and -0.676 e.Å-3

(A)

Bond	Bond lengths Å	Bond	Bond Lengths Å
		N(1)-Ag(1)-N(5)	142.11(7)
Ag(1)-N(1)	2.1643(19)	N(1)-Ag(1)-N(3)	119.06(7)
Ag(1)-N(5)	2.2516(19)	N(5)-Ag(1)-N(3)	97.04(7)
Ag(1)-N(3)	2.3279(19)	N(1)-Ag(1)-Ag(1)#1	91.86(5)
Ag(1)-Ag(1)#1	3.3064(5)	N(5)-Ag(1)-Ag(1)#1	80.63(5)
Ag(2)-N(4)#1	2.142(2)	N(3)-Ag(1)-Ag(1)#1	116.97(5)
Ag(2)-N(6)	2.2410(19)	N(4)#1-Ag(2)-N(6)	150.30(7)
Ag(2)-N(2)	2.3705(19)	N(4)#1-Ag(2)-N(2)	117.89(7)
	91.81(7)	N(6)-Ag(2)-N(2)	91.81(7)

(B)

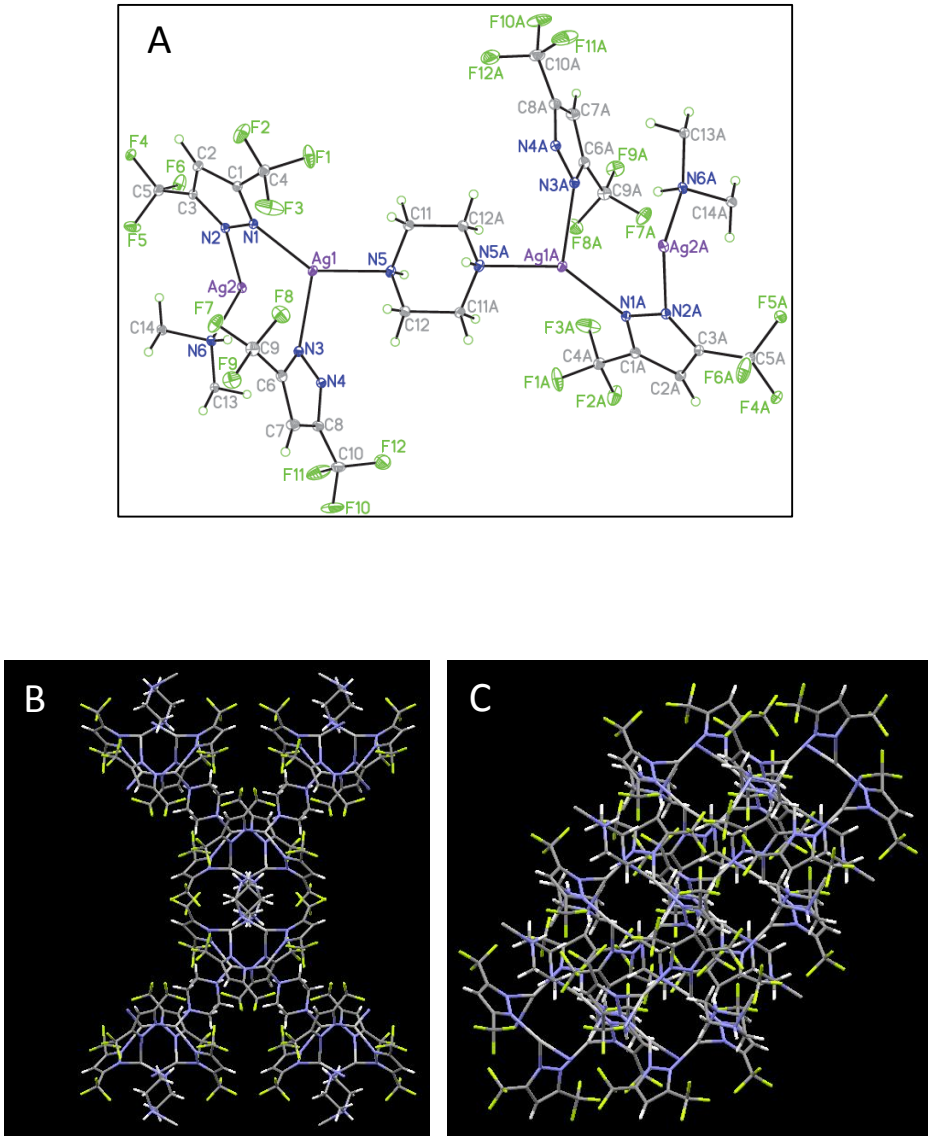

Fig. 25 Molecular structure (A) and packing (B and C) diagrams from the crystal structure of {[3,5-$(CF_3)_2$Pz]Ag}$_4$ppz showing extended polymeric porous phase.

2.3.3.2. Absorption spectra

Figure 26 shows intense absorption bands for {[3,5-$(CF_3)_2$Pz]Ag}$_4$ppz in the UV region due to ligand charge π-π*.

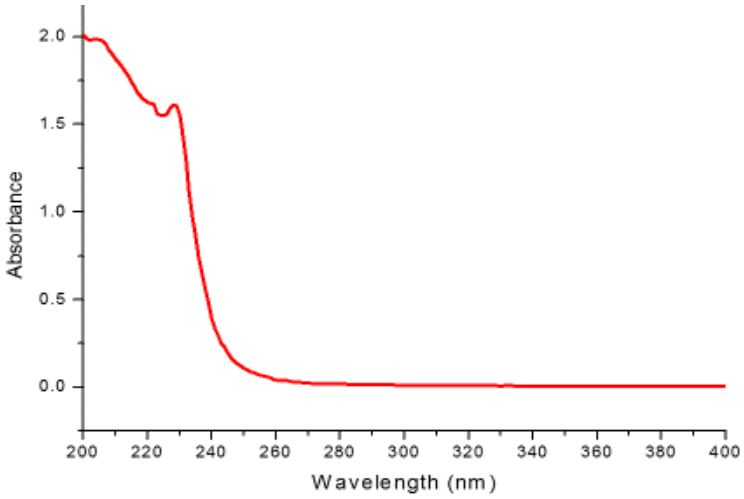

Fig. 26 The absorption spectrum of {[3,5-$(CF_3)_2$Pz]Ag}$_4$ppz in acetonitrile at RT

2.3.3.3. Characterization using ^{1}HNMR, TGA, FT-IR spectra

^{1}H NMR measurements of {[3,5-$(CF_3)_2$Pz]Ag}$_4$ppz were done by using deuterated acetone. Here we are illustrating the ^{1}H NMR spectra of {[3,5-$(CF_3)_2$Pz]Ag}$_4$ppz. As expected, the proton NMR spectra of the fluorinated silver pyrazolates lack the broad peak corresponding to the C-H proton of the pyrazoles at around δ = 7.0 [13]. However, the ^{1}H NMR signal corresponding to the protons at pyrazolyl ring 4-position shows a small downfield shift. Figure 27 represents the ^{1}H NMR spectrum of {[3,5-$(CF_3)_2$Pz]Ag}$_4$ppz. The sharp peaks at δ= 2.85 and 1.90 are assigned to piperazine (ppz).

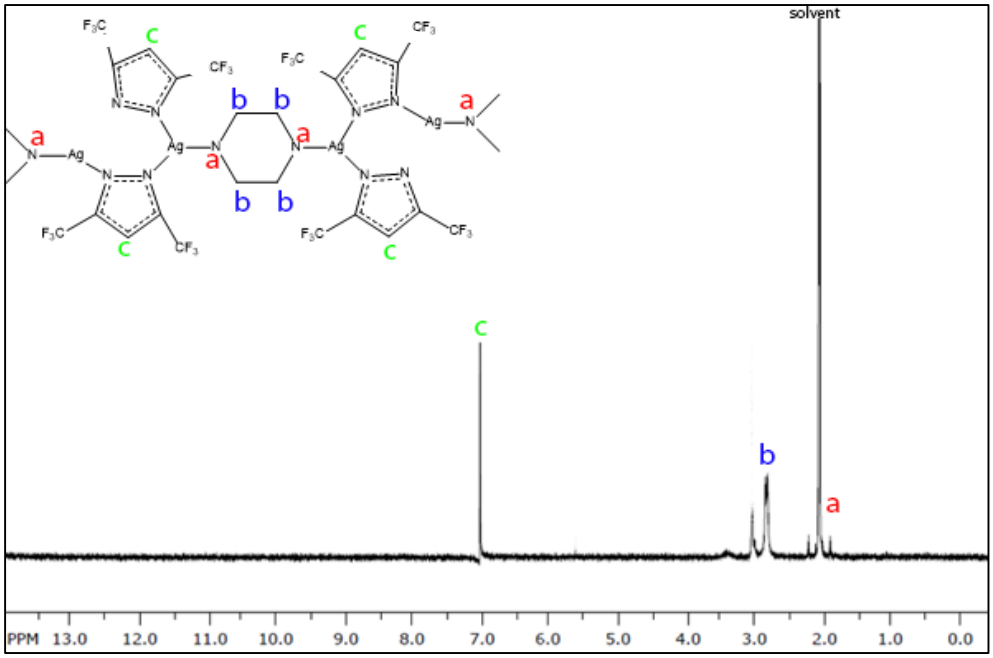

Fig. 27 ^{1}H NMR (400 MHz) spectrum of {[3,5-$(CF_3)_2$Pz]Ag}$_4$ppz in Acetone d_6

The product {[3,5-$(CF_3)_2$Pz]Ag}$_4$ppz has a formula structure (C_{28} H_{20} Ag_4 F_{24} N_{12}: MW: 1412.04g/mol). Ag_4 weight %= (107.86*4/1412.04)x100= 30.55%. Theoretically, there is 30.55% of silver in 1412.04 g/mole. TGA (Q50 V6.7) analysis in figure 28 shows that 58.27% weight loss of the organic ligands in {[3,5-$(CF_3)_2$Pz]Ag}$_4$ppz. It indicates that the silver is left from the remaining percentage of 41.73%, which is much higher than the theoretical percentage.

The IR spectra for {[3,5-$(CF_3)_2$Pz]Ag}$_4$ppz, shown in figure 29, confirms the presence of the ligands (Pz, ppz) in the product.

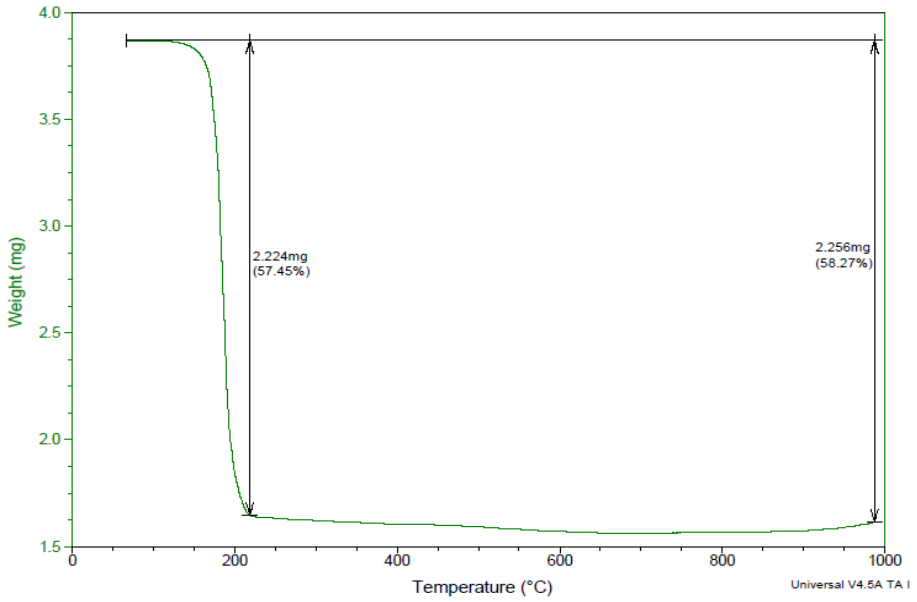

Fig 28. TGA (Q50 V6.7) analysis of {[3,5-$(CF_3)_2$Pz]Ag}$_4$ppz

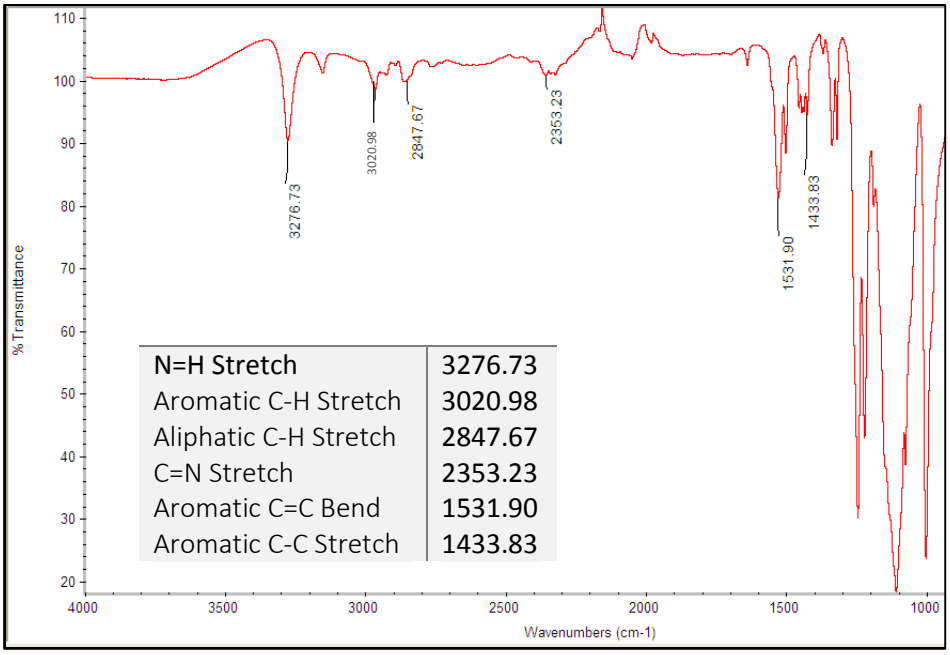

Fig. 29 FT-IR spectrum of {[3,5-$(CF_3)_2$Pz]Ag}$_4$ppz

2.4 Results and discussion for copper complexes

Copper complexes: $\{[3,5\text{-}(CF_3)_2Pz]Cu\}_n$ bpe_n and $\{[3,5\text{-}(CF_3)_2Pz]Cu\}_n$ ppz_n were prepared by treatment of trinuclear copper (I) complex with a slight molar excess of the corresponding linear bridging diimine ligands in benzene. They were obtained in high yields (>80%). Copper complexes are air sensitive crystalline solids. They are soluble in organic solvents such as acetonitrile, acetone and tetrahydrofuran. Although we couldn't get crystal structures from both complexes, we were able to characterize them by using absorption spectroscopy, ^{1}HNMR spectroscopy, TGA, and FT-IR spectroscopy. Both copper complexes have no luminescence. In this section we will discuss the ^{1}HNMR spectra, FT-IR, TGA and absorption properties of both copper metal complexes.

2.4.1. $\{[3,5\text{-}(CF_3)_2Pz]Cu\}_n$ bpe_n

2.4.1.1. Absorption spectra

Figures 30, 31, and 32 show intense absorption of $\{[3,5\text{-}(CF_3)_2Pz]Cu\}_n$ bpe_n bands in the UV-Visible region due to ligand charge π-π*. The following figures show the absorption and molar absorptivity spectra of $\{[3,5\text{-}(CF_3)_2Pz]Cu\}_n$ bpe_n (1:1), (1:2) and (1:6) at high concentration and at $1X10^{-5}$M.

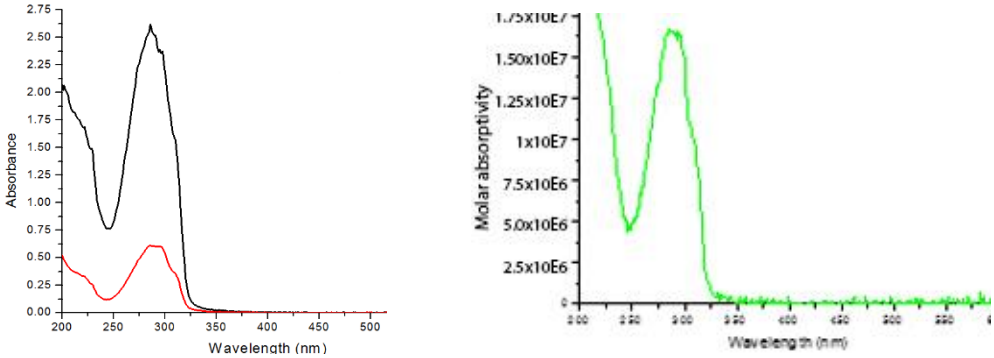

Fig. 30 The absorption spectrum at high concentration (left) and the molar absorptivity spectrum of $\{[3,5\text{-}(CF_3)_2Pz]Cu\}_n\,bpe_n$ (1:1) in acetonitrile at $1x10^{-5}$M (right).

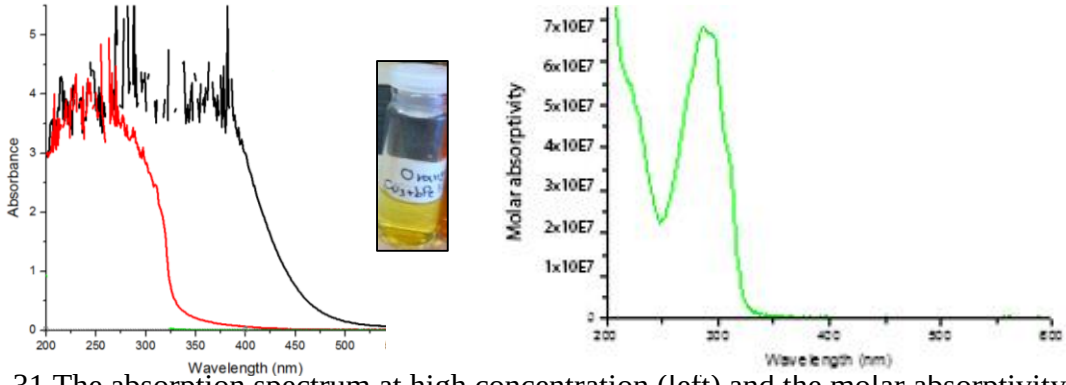

Fig. 31 The absorption spectrum at high concentration (left) and the molar absorptivity spectrum of $\{[3,5\text{-}(CF_3)_2Pz]Cu\}_n\,bpe_n$ (1:2) in acetonitrile at $1x10^{-5}$M (right).

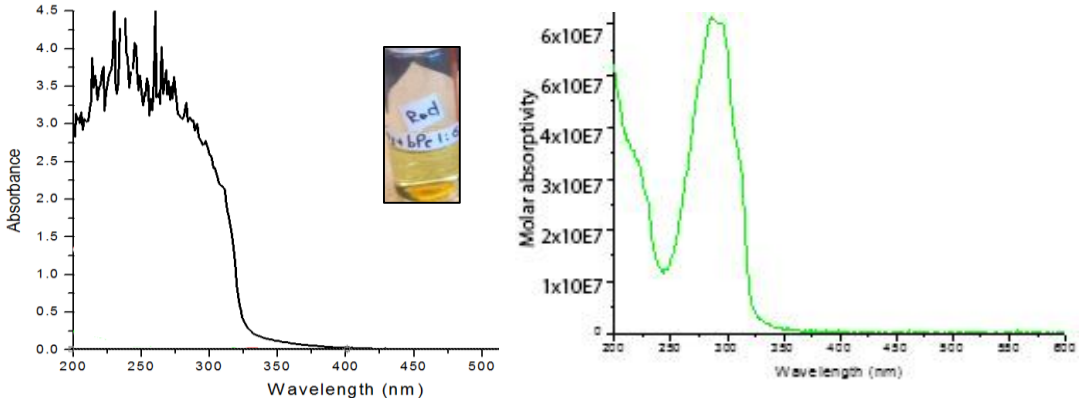

Fig. 32 The absorption spectrum at high concentration (left) and the molar absorptivity spectrum of $\{[3,5\text{-}(CF_3)_2Pz]Cu\}_n\,bpe_n$ (1:6) in acetonitrile at $1x10^{-5}$M (right).

2.4.1.2. Characterization using ^{1}HNMR, TGA, FT-IR spectra

^{1}HNMR measurements of $\{[3,5\text{-}(CF_3)_2Pz]Cu\}_n$ bpe_n were done by using deuterated dichloromethane. Here we are illustrating the ^{1}HNMR spectra of $\{[3,5\text{-}(CF_3)_2Pz]Cu\}_n$ bpe_n. As expected, the proton NMR spectra of the fluorinated copper pyrazolates lack the broad peak corresponding to the C-H proton of the pyrazoles at around δ = 7.0 [13]. However, the ^{1}H NMR signal corresponding to the protons at pyrazolyl ring 4-position shows a small downfield shift. Figure 33 represents the ^{1}H NMR spectrum of $\{[3,5\text{-}(CF_3)_2Pz]Cu\}_n$ bpe_n. The sharp peaks at δ = 7.42, 8.51 are assigned to 1,2-bis(4-pyridyl) ethylene (bpe).

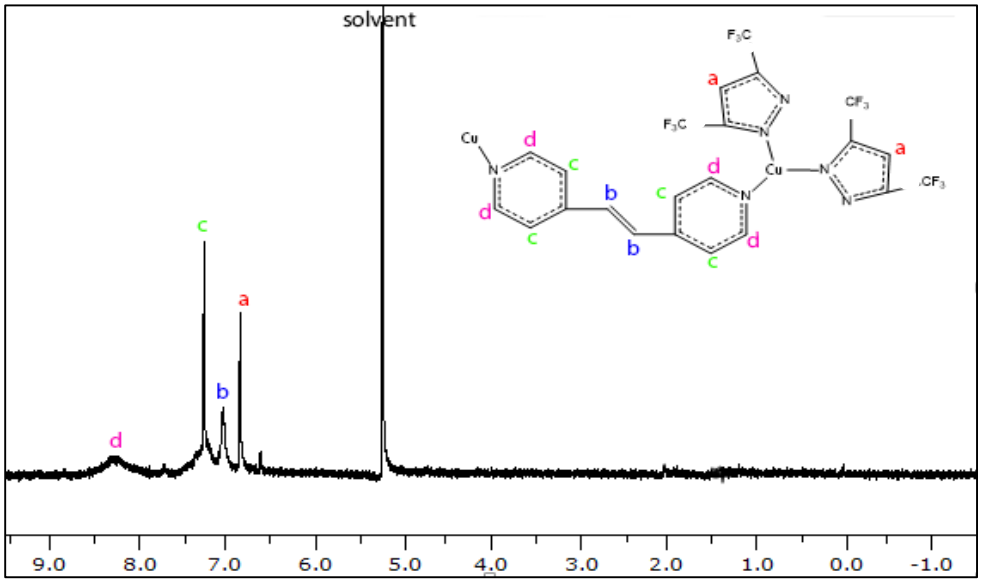

Fig. 33 ^{1}H NMR (400 MHz) spectrum of Cu-Pz-bpe in CD_2Cl_2 with a predicted structure.

The expected percentage of the copper in $\{[3,5\text{-}(CF_3)_2Pz]Cu\}_n\,bpe_n$ is around 20%. However, TGA (Q50 V6.7) analysis in figure 34 shows 91.45% weight loss of the organic ligands in $\{[3,5\text{-}(CF_3)_2Pz]Cu\}_n\,bpe_n$. It indicates that the copper is left from the remaining percentage of 8.65%, which leads to a high possibility of copper sublimation.

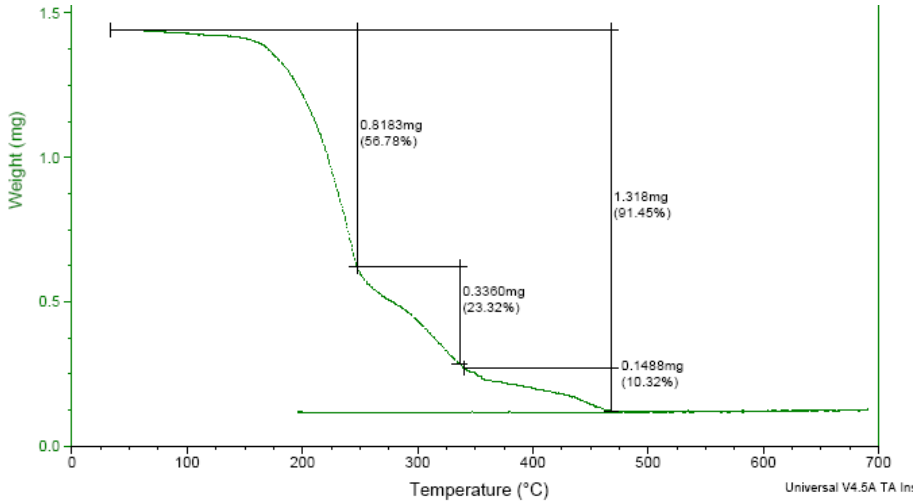

Fig. 34 TGA (Q50 V6.7) analysis of $\{[3,5\text{-}(CF_3)_2Pz]Cu\}_n\,bpe_n$.

The IR spectra for $\{[3,5\text{-}(CF_3)_2Pz]Cu\}_n\,bpe_n$, shown in figure 35, confirms the presence of the ligands (Pz, bpe) in the product.

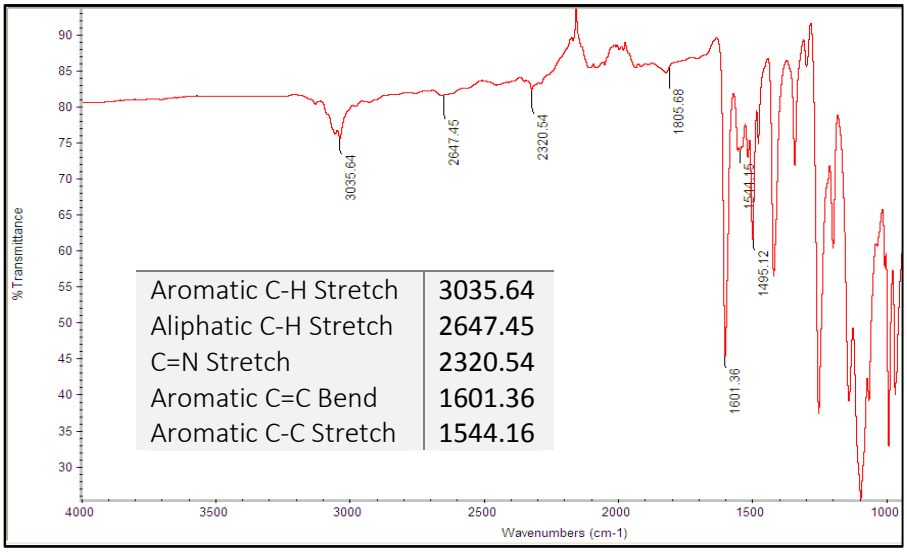

Fig. 35 FT-IR spectrum of $\{[3,5\text{-}(CF_3)_2Pz]Cu\}_n\,bpe_n$.

2.4.2. {[3,5-$(CF_3)_2$Pz]Cu}$_n$ ppz$_n$

2.4.2.1. Absorption spectra

Figure 36 shows intense absorption of {[3,5-$(CF_3)_2$Pz]Cu}$_n$ ppz$_n$ bands in the UV-Visible region due to ligand charge π-π*.

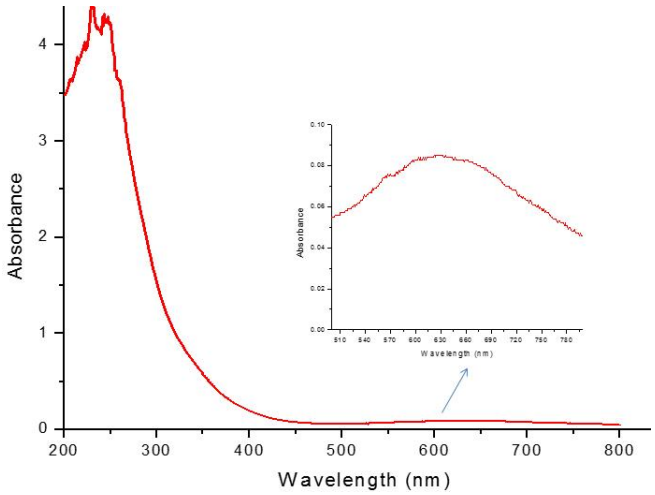

Fig. 36 The absorption spectrum of Cu-Pz-ppz in acetonitrile.

2.4.1.2. Characterization using ^{1}HNMR, TGA, FT-IR spectra

^{1}HNMR measurements of {[3,5-$(CF_3)_2$Pz]Cu}$_n$ ppz$_n$ were done by using deuterated acetone. Here we are illustrating the ^{1}HNMR spectra of {[3,5-$(CF_3)_2$Pz]Cu}$_n$ ppz$_n$. As expected, the proton NMR spectra of the fluorinated copper pyrazolates lack the broad peak corresponding to the C-H proton of the pyrazoles at around δ = 7.0 [13]. However, the ^{1}H NMR signal corresponding to the protons at pyrazolyl ring 4-position shows a small downfield shift. Figure 37 represents the ^{1}H NMR spectrum of {[3,5-$(CF_3)_2$Pz]Cu}$_n$ ppz$_n$. The sharp peaks at δ = 2.6, 1.9 are assigned to piperazine (ppz).

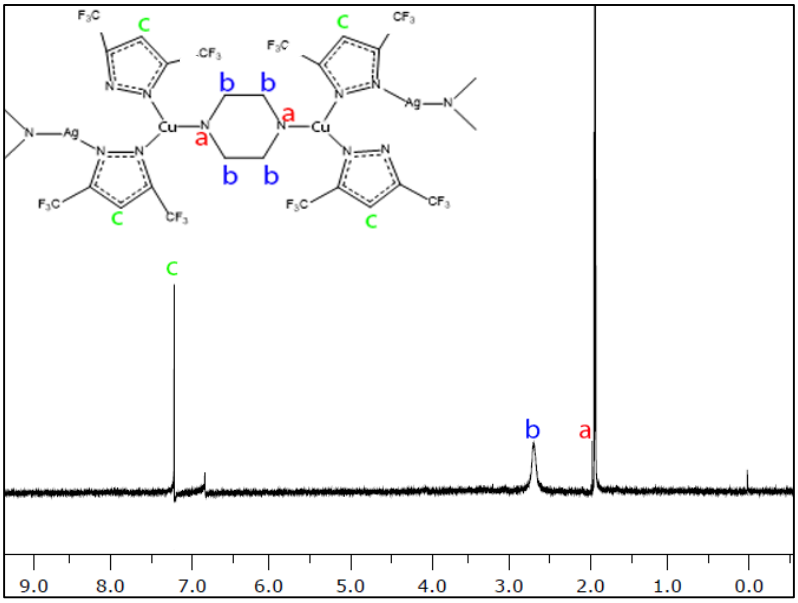

Fig. 37 ^{1}H NMR (400 MHz) spectrum of $\{[3,5\text{-}(CF_3)_2Pz]Cu\}_n\ ppz_n$ in Acetone d_6 with a predicted structure.

The expected percentage of the copper in $\{[3,5\text{-}(CF_3)_2Pz]Cu\}_n\ ppz_n$ is around 20%. However, TGA (Q50 V6.7) analysis in figure 38 shows 92.17% weight loss of the organic ligands in $\{[3,5\text{-}(CF_3)_2Pz]Cu\}_n\ ppz_n$. It indicates that the copper is left from the remaining percentage of 7.93%. The low percentage is probably due copper sublimation. The IR spectra for $\{[3,5\text{-}(CF_3)_2Pz]Cu\}_n\ ppz_n$, shown in figure 39, confirms the presence of the ligands (Pz, ppz) in the product.

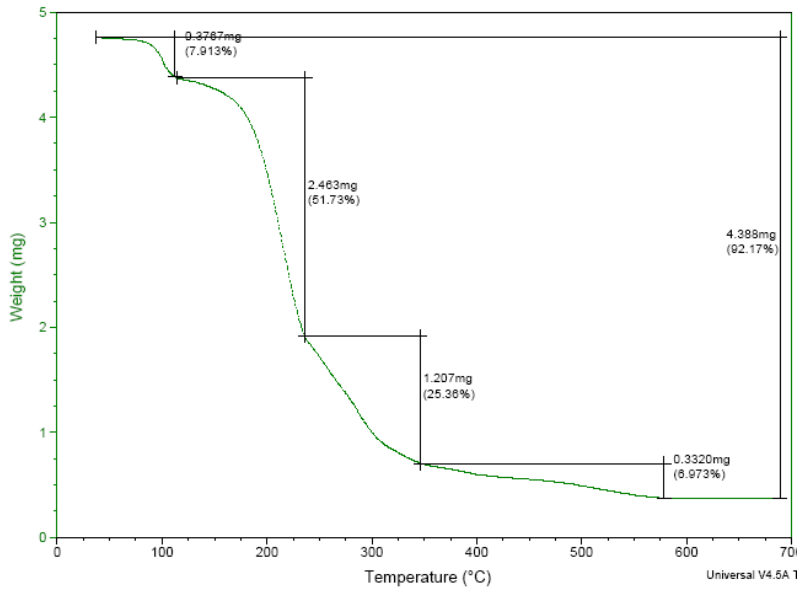

Fig. 38 TGA (Q50 V6.7) analysis of $\{[3,5\text{-}(CF_3)_2Pz]Cu\}_n$ ppz_n

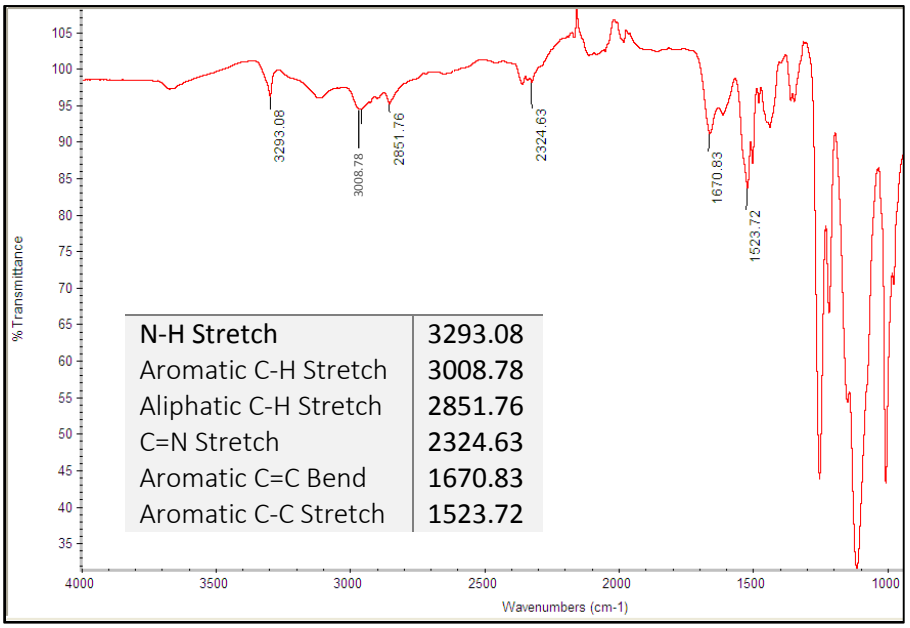

Fig. 39 FT-IR spectrum of $\{[3,5\text{-}(CF_3)_2Pz]Cu\}_n$ ppz_n

2.5 Results and discussion for mixed metal complexes

Mixed metal complexes: $\{[3,5\text{-}(CF_3)_2Pz]AgCu\}_2bpa_2$, $\{[3,5\text{-}(CF_3)_2Pz]AgCu\}_n\ bpe_n$ and $\{[3,5\text{-}(CF_3)_2Pz]AgCu\}_n\ ppz_n$ were prepared by treatment of mixing trinuclear copper (I) and silver (I) complexes with a slight molar excess of the corresponding linear bridging diimine ligands in benzene. They were obtained in high yields (>80%). Mixed metal complexes are air sensitive crystalline solids. We could get crystal structure from $\{[3,5\text{-}(CF_3)_2Pz]AgCu\}_2bpa_2$, but we couldn't get crystal structures from the other complexes; $\{[3,5\text{-}(CF_3)_2Pz]AgCu\}_n\ bpe_n$ and $\{[3,5\text{-}(CF_3)_2Pz]AgCu\}_n\ ppz_n$. In this section we will discuss the photoluminescence spectra of $\{[3,5\text{-}(CF_3)_2Pz]AgCu\}_2bpa_2$, absorption properties ^{1}HNMR spectra, TGA, and FT-IR of all mixed metal complexes.

2.5.1. $\{[3,5\text{-}(CF_3)_2Pz]AgCu\}_2bpa_2$

2.5.1.1. The X-ray crystallographic data

In this section, we will discuss in details the x-ray crystallographic data. Based on table 4, the crystals obtained in $\{[3,5\text{-}(CF_3)_2Pz]AgCu\}_2bpa_2$ have the p-1space group with a = 10.2420 (4) Å, b = 11.8402 (4) Å, c = 14.8085 (5) Å, α= 3.8430(10)°, β = 96.9770(10)°, and γ = 96.3040(10)°. *$\{[3,5\text{-}(CF_3)_2Pz]AgCu\}_2bpa_2$* crystallizes in triclinic system as a dimer, and with one molecule in the asymmetric unit (for a Z value of 2). The dimers sit on an inversion center. Figure 40(A) shows 4-coordinate silver and copper interconnected dimeric units with 0.70 and 1.3 probabilities for silver and copper, respectively. Silver (I) and Copper (I) coordinate with a nitrogen from a pyrazole and from 1,2-bis(4-

pyridyl)ethane. The backing structures in figures 40(B and C) reveal on extended chains with large porosity. All the non-hydrogen atoms were refined anisotropically. The hydrogen atoms were placed at calculated positions and refined using a riding model. The final full-matrix least-squares refinement on *F*2 gave R1:4.38% and wR2:7.98% for all data. The goodness-of-fit was 1.029. Table 4(B) shows selected bond distances (Å) and angles (°) for $\{[3,5\text{-}(CF_3)_2Pz]AgCu\}_2bpa_2$.

Table 4

(A) X-ray Crystallographic Data for $\{[3,5\text{-}(CF_3)_2Pz]AgCu\}_2bpa_2$, (B) Selected bond distances (Å) and angles (°) for $\{[3,5\text{-}(CF_3)_2Pz]AgCu\}_2bpa_2$

Empirical Formula	**C34 H26 AG0.69 CU1.31 F12 N8**
Formula Weight	932.30
Temperature	100(2) K
Wavelength	0.71073 Å
Crystal System	Triclinic
Space Group	P -1
Unit Cell Dimensions	a = 10.2420(4) Å, α= 3.8430(10)°.b = 11.8402(4) Å, β= 96.9770(10)°.c = 14.8085(5) Å, γ = 96.3040(10)°.
Volume	1765.82(11) $Å^3$
Z	2
Density (Calculated)	1.753 Mg/m^3
Absorption Coefficient	1.274 mm^{-1}
F(000)	929
Crystal Size	0.17 x 0.09 x 0.08 mm^3
Theta Range For Data Collection	1.74 to 27.13°
Index Ranges	-13<=h<=13, -15<=k<=15, -18<=l<=18
Reflections Collected	24266
Independent Reflections	7780 [R(int) = 0.0275]
Completeness To Theta =2 7.12°	99.9%
Absorption Correction	Semi-empirical from equivalents
Max. And Min. Transmission	0.9082 and 0.8163
Refinement Method	Full-matrix least-squares on F^2
Data / Restraints / Parameters	7780 / 0 / 512
Goodness-Of-Fit On F^2	1.029
Final R Indices [I>2sigma(I)]	R1 = 0.0338, wR2 = 0.0751
R Indices (All Data)	R1 = 0.0438, wR2 = 0.0798

(A)

Table 4. Cont'd

Bond	Bond Lengths Å	Bond	Bond Lengths Å
Ag(1)-N(1)	2.031(10)	Cu(1)-N(6)	2.110(8)
Ag(1)-N(5)	2.151(10)	Cu(1)-N(1)	2.125(9)
Ag(1)-N(6)	2.224(10)	Cu(1)-N(3)	2.155(9)
Ag(1)-N(3)	2.248(10)	Cu(1)-N(5)	2.235(9)
Ag(2)-N(7)	2.015(8)	Cu(2)-N(4)	2.114(7)
Ag(2)-N(4)	2.038(9)	Cu(2)-N(2)	2.152(7)
Ag(2)-N(2)	2.319(8)	Cu(2)-N(8)	2.173(7)
Ag(2)-N(8)	2.349(8)	Cu(2)-N(7)	2.177(7)

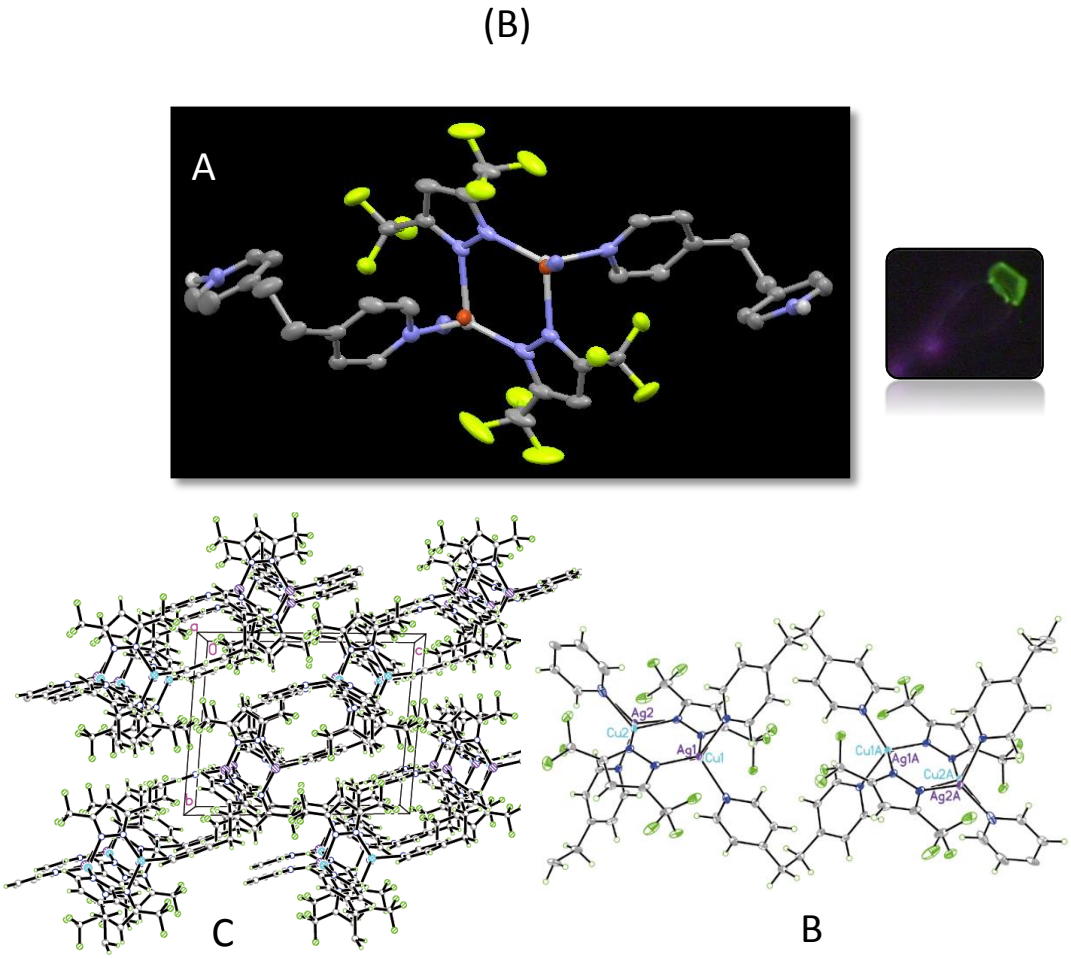

Fig. 40 Molecular structure (A) and packing (B and C) diagrams from the crystal structure of $\{[3,5\text{-}(CF_3)_2Pz]AgCu\}_2bpa_2$ showing extended polymeric porous phase.

2.5.1.2. Photoluminescence and absorption spectra

The complex $\{[3,5\text{-}(CF_3)_2Pz]AgCu\}_2bpa_2$ exhibited yellow-green photoluminescence (PL) in the solid state at room temperature (RT) and 77K. However, it didn't exhibit any (PL) in solution. The emission spectra and lifetime at RT and 77K are shown in figures 41, 42. The emission band, with maximum at λ_{em}= 558 nm, was observed for the solid (powder) at RT. Upon cooling to 77K, an emission band, with maximum at 570 nm, was observed. The RT emission lifetime is 9.77 μs, while the 77K emission lifetime is 13.19 μs, which are all suggesting phosphorescence from a triplet excited state. Intense absorption bands shown in figure 43 for $\{[3,5\text{-}(CF_3)_2Pz]AgCu\}_2bpa_2$ in the UV-Visible region due to ligand charge π-π*.

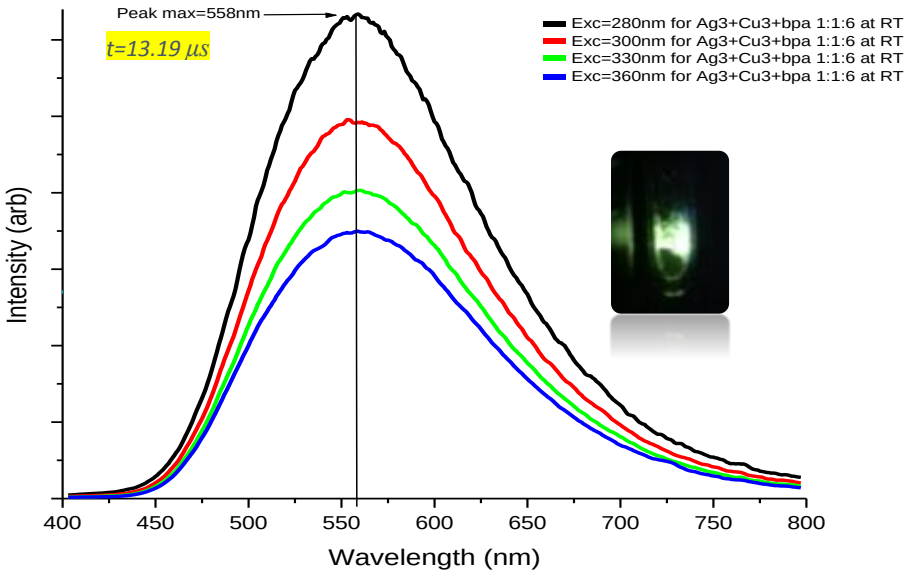

Fig. 41 Photoluminescence emission spectra of $\{[3,5\text{-}(CF_3)_2Pz]AgCu\}_2bpa_2$ in a solid state at different excitations at RT.

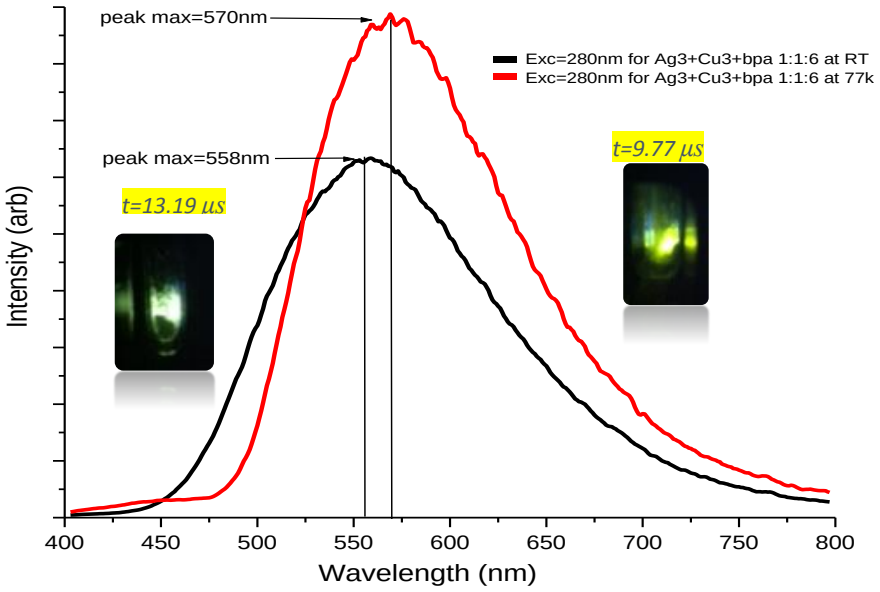

Fig. 42 Comparison between emission spectra of {[3,5-$(CF_3)_2$Pz]AgCu}$_2$bpa$_2$ at RT and at 77K.

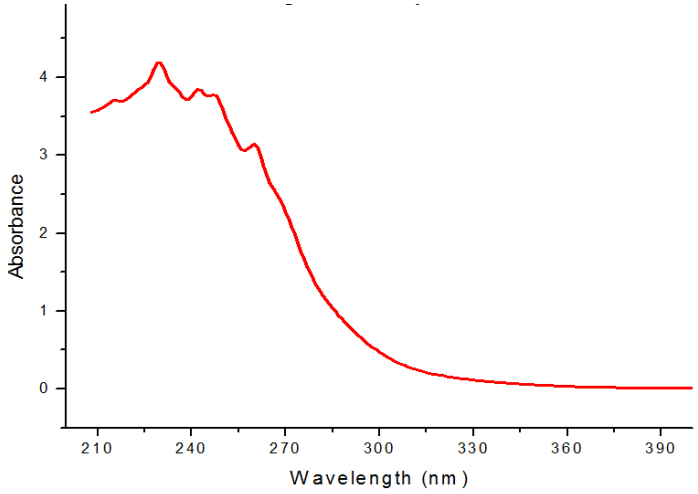

Fig. 43 The absorption spectrum of {[3,5-$(CF_3)_2$Pz]AgCu}$_2$bpa$_2$ in acetonitrile.

2.5.1.3. Characterization using ^{1}HNMR, TGA, FT-IR spectra

^{1}H NMR measurements of {[3,5-$(CF_3)_2$Pz]AgCu}$_2$bpa$_2$ were done by using deuterated acetone. Here we are illustrating the ^{1}H NMR spectra of {[3,5-$(CF_3)_2$Pz]AgCu}$_2$bpa$_2$. As expected, the proton NMR spectra of the fluorinated coinage metal pyrazolates lack the broad peak corresponding to the C-H proton of the pyrazoles at around δ = 7.0 [13]. However, the ^{1}H NMR signal corresponding to the protons at pyrazolyl ring 4-position shows a small downfield shift. Figure 44 represents the ^{1}H NMR spectrum of {[3,5-$(CF_3)_2$Pz]AgCu}$_2$bpa$_2$. The sharp peaks at δ = 7.24, 8.56 and 2.92 are assigned to 1,2-bis(4-pyridyl)ethane (bpa).

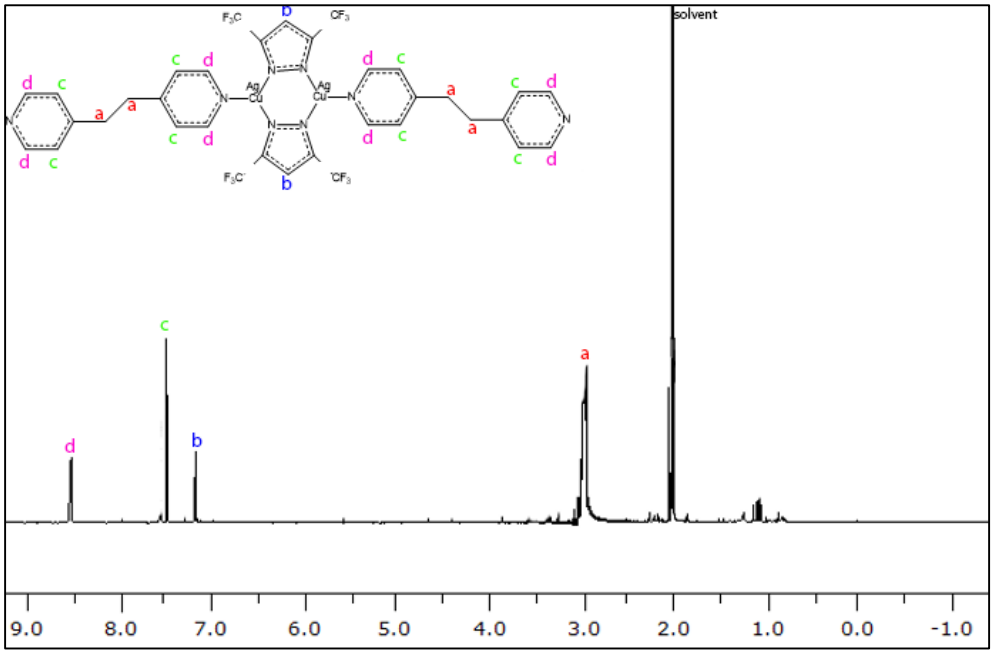

Fig. 44 ^{1}H NMR (400 MHz) spectrum of {[3,5-$(CF_3)_2$Pz]AgCu}$_2$bpa$_2$ in Acetone d_6

The product $\{[3,5\text{-}(CF_3)_2Pz]AgCu\}_2bpp_2$ has a formula structure ($C_{34}H_{26}Ag_{0.69}Cu_{1.31}F_{12}N_8$: MW: 932.30g/mol). Ag_2 weight %= (107.86*0.69+63.54*1.31/819.15)x100= 19.24%. Theoretically, there is 19.24% silver in 819.15 g/mole. TGA (Q50 V6.7) analysis in figure 45 shows that 88.14% weight loss of the organic ligands in the $\{[3,5\text{-}(CF_3)_2Pz]AgCu\}_2bpp_2$ product. It indicates that Ag/Cu mixed-metal composition is left from the remaining percentage of 11.86%, which is less than the theoretical weight calculations based on the crystallographic empirical formula. The difference between the theoretical percentage and the actual percentage is probably due to impurities or solvents in the sample (powder). The IR spectra for $\{[3,5\text{-}(CF_3)_2Pz]AgCu\}_2bpa_2$, shown in figure 46, confirms the presence of the ligands (Pz, bpa) in the product.

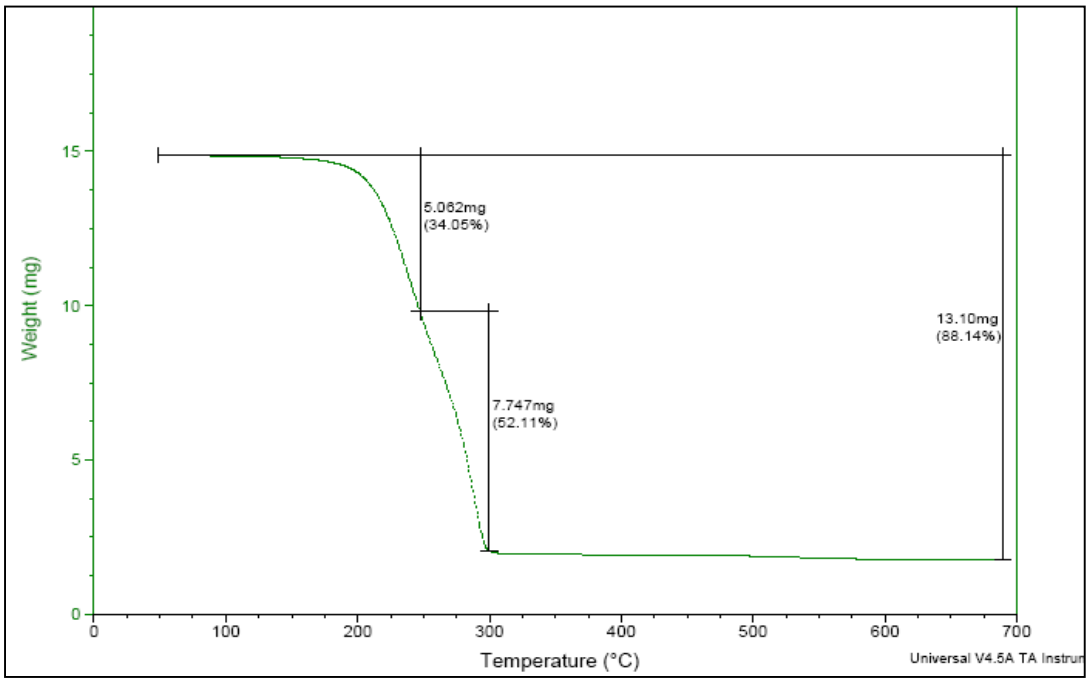

Fig. 45 TGA (Q50 V6.7) analysis of $\{[3,5\text{-}(CF_3)_2Pz]AgCu\}_2bpp_2$

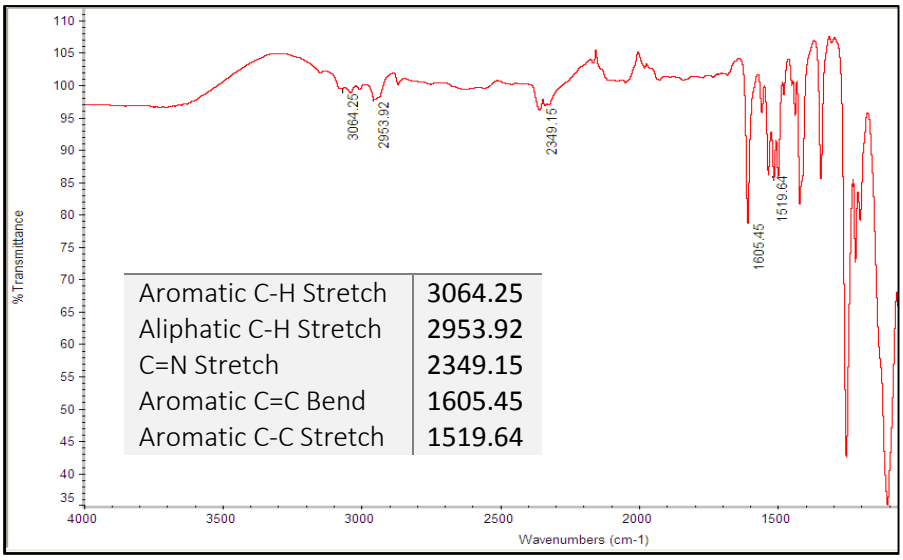

Fig. 46 FT-IR spectrum of $\{[3,5\text{-}(CF_3)_2Pz]AgCu\}_2bpa_2$.

2.5.2. $\{[3,5\text{-}(CF_3)_2Pz]AgCu\}_n\, bpe_n$

2.5.2.1. Absorption spectra

Intense absorption bands shown in figure 47 for $\{[3,5\text{-}(CF_3)_2Pz]AgCu\}_n\, bpe_n$ in the UV-Visible region due to ligand charge π-π*.

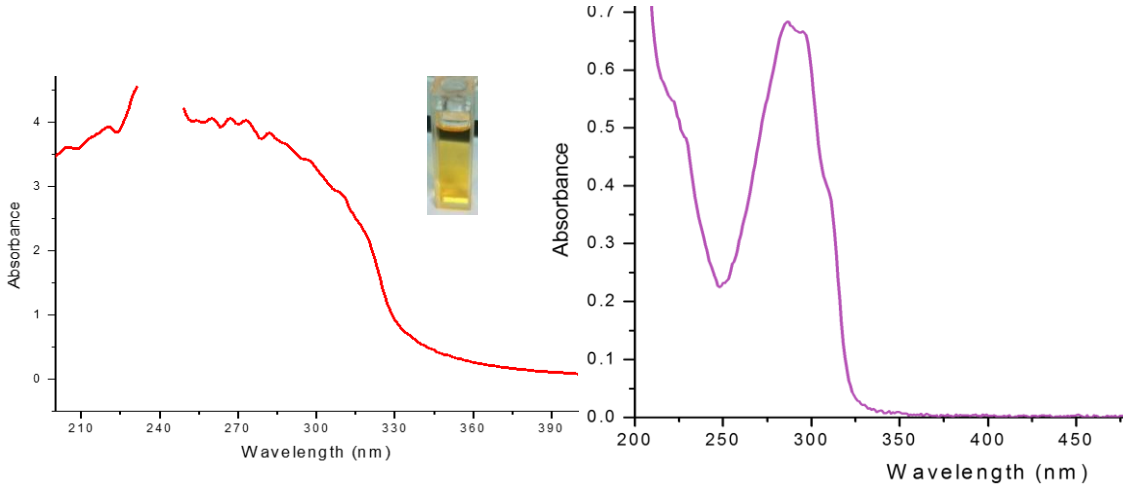

Fig. 47 The absorption spectrum of $\{[3,5\text{-}(CF_3)_2Pz]AgCu\}_n\, bpe_n$ (1:1:6) in acetonitrile at high concentration (left) and at $1x10^{-5}$M (right).

2.5.2.2. Characterization using ^{1}HNMR, TGA, FT-IR spectra

^{1}HNMR measurements of $\{[3,5\text{-}(CF_3)_2Pz]AgCu\}_n\,bpe_n$ were done by using deuterated acetone. Here we are illustrating the ^{1}HNMR spectra of $\{[3,5\text{-}(CF_3)_2Pz]AgCu\}_n\,bpe_n$. As expected, the proton NMR spectra of the fluorinated copper pyrazolates lack the broad peak corresponding to the C-H proton of the pyrazoles at around $\delta = 7.0$ [13]. However, the ^{1}H NMR signal corresponding to the protons at pyrazolyl ring 4-position shows a small downfield shift. Figure 48 represents the ^{1}H NMR spectrum of $\{[3,5\text{-}(CF_3)_2Pz]AgCu\}_n\,bpe_n$. The sharp peaks at $\delta = 7.02$ and 7.6 are assigned to 1,2-bis(4-pyridyl) ethylene (bpe).

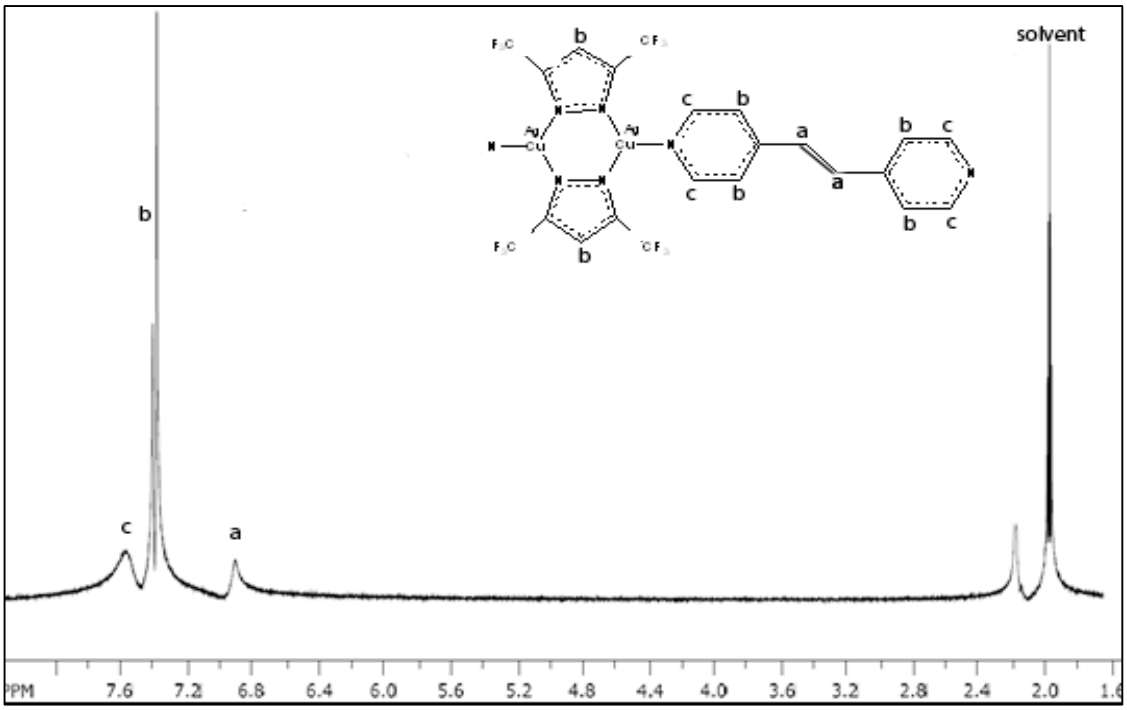

Fig. 48 ^{1}H NMR (400 MHz) spectrum of $\{[3,5\text{-}(CF_3)_2Pz]AgCu\}_n\,bpe_n$ in Acetone d_6 with a predicted structure.

The expected percentage of the mixed metal Ag and Cu in $\{[3,5\text{-}(CF_3)_2Pz]AgCu\}_n\,bpe_n$ is around 20%. TGA (Q50 V6.7) analysis in figure 49 shows 91.36% weight loss of the organic ligands in $\{[3,5\text{-}(CF_3)_2Pz]AgCu\}_n\,bpe_n$. It indicates that Ag/Cu mixed-metal composition is left from the remaining percentage of 8.74%. The low percentage is probably due to copper sublimation. IR spectra for $\{[3,5\text{-}(CF_3)_2Pz]AgCu\}_n\,bpe_n$, shown in figure 50, confirms the presence of the ligands (Pz, bpe) in the product.

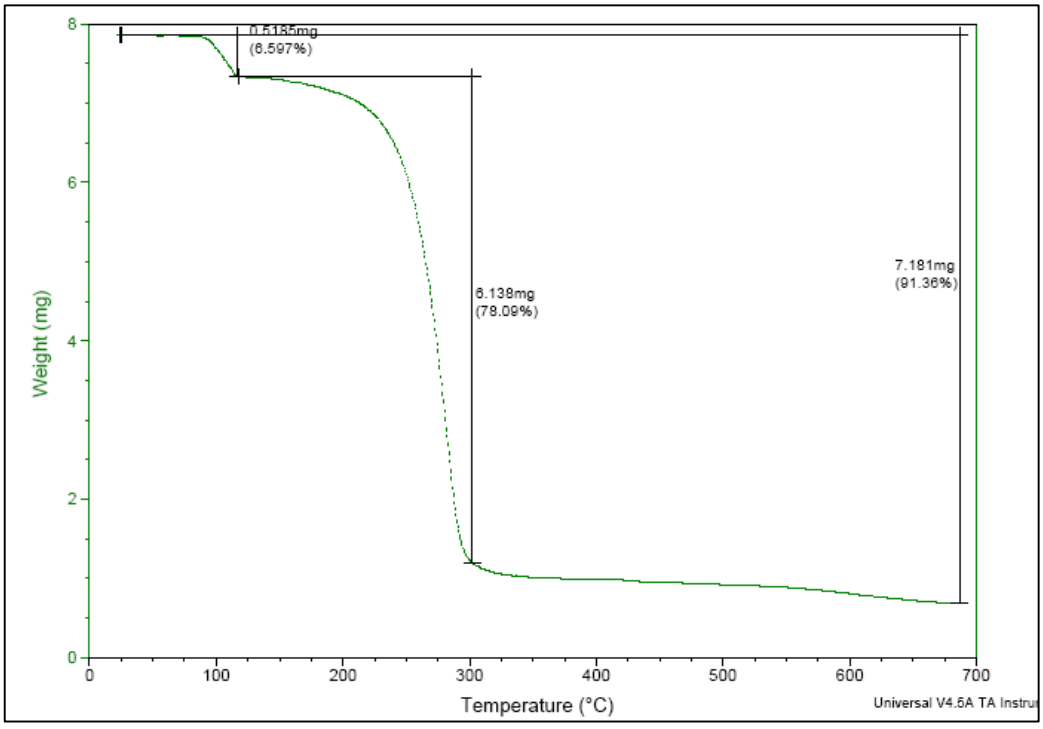

Fig. 49 TGA (Q50 V6.7) analysis of $\{[3,5\text{-}(CF_3)_2Pz]AgCu\}_n\,bpe_n$

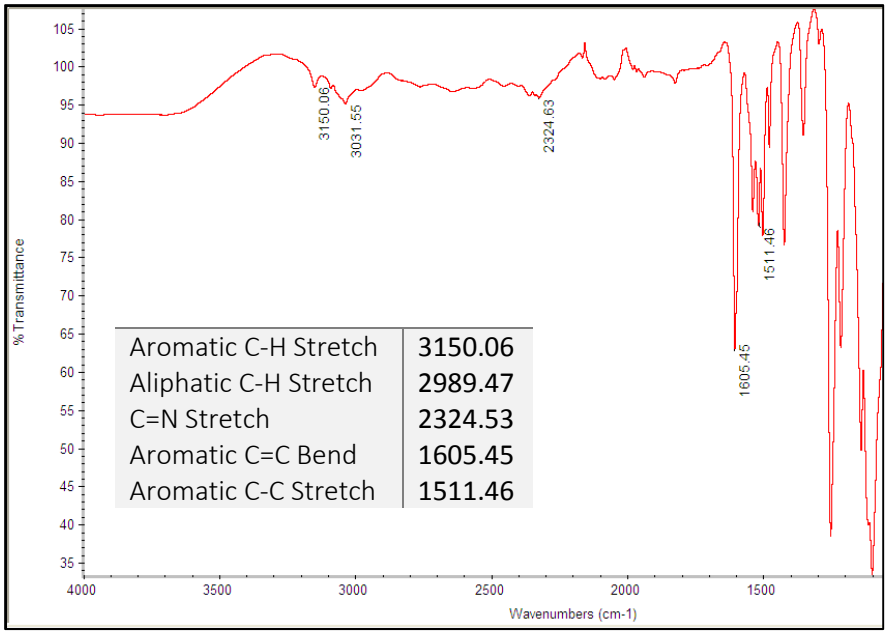

Fig. 50 FT-IR spectrum of $\{[3,5\text{-}(CF_3)_2Pz]AgCu\}_n\ bpe_n$

2.5.3. $\{[3,5\text{-}(CF_3)_2Pz]AgCu\}_n\ ppz_n$

2.5.3.1. Absorption spectra

Figure 51 shows intense absorption bands of $\{[3,5\text{-}(CF_3)_2Pz]AgCu\}_n\ ppz_n$ in the UV-Visible region due to ligand charge π-π*.

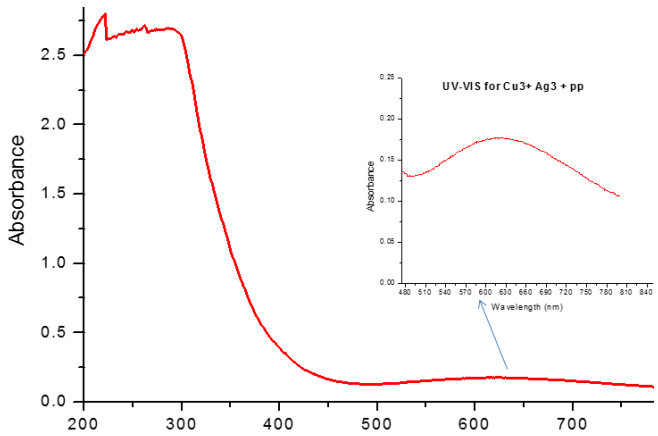

Fig. 51 The absorption spectrum of $\{[3,5\text{-}(CF_3)_2Pz]AgCu\}_n\ ppz_n$ (1:6) in acetonitrile.

2.5.3.2. Characterization using ^{1}HNMR, TGA, FT-IR spectra

^{1}HNMR measurements of $\{[3,5\text{-}(CF_3)_2Pz]AgCu\}_n$ ppz_n were done by using deuterated acetone. Here we are illustrating the ^{1}HNMR spectra of $\{[3,5\text{-}(CF_3)_2Pz]AgCu\}_n$ ppz_n. As expected, the proton NMR spectra of the fluorinated copper pyrazolates lack the broad peak corresponding to the C-H proton of the pyrazoles at around $\delta = 7.0$ [13].However, the ^{1}H NMR signal corresponding to the protons at pyrazolyl ring 4-position shows a small downfield shift. Figure 52 represents the ^{1}H NMR spectrum of $\{[3,5\text{-}(CF_3)_2Pz]AgCu\}_n$ ppz_n. The sharp peaks at $\delta = 2.22$ and 1.90 are assigned to piperazine (ppz).

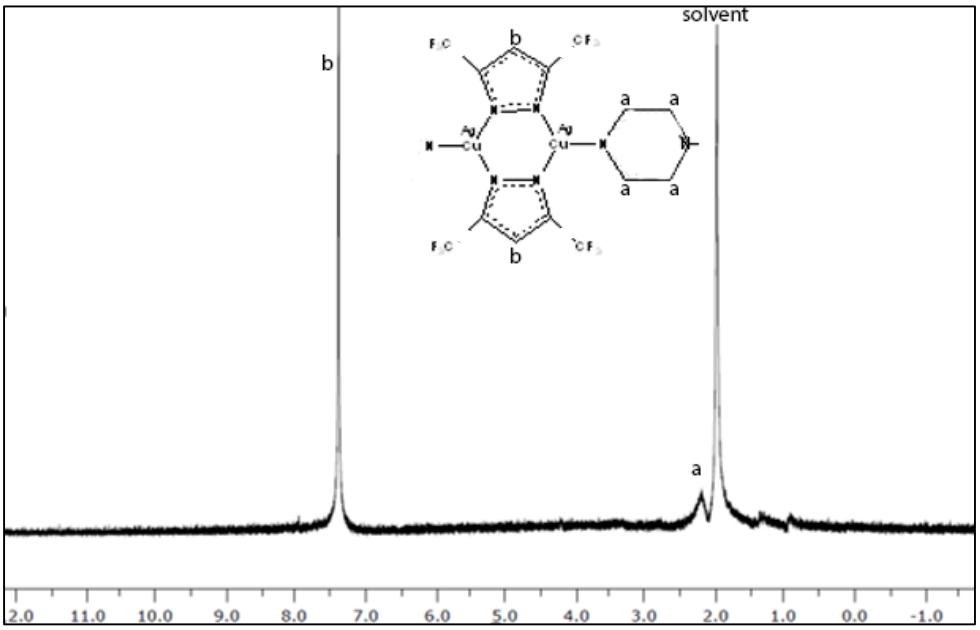

Fig. 52 ^{1}H NMR (400 MHz) spectrum of $\{[3,5\text{-}(CF_3)_2Pz]AgCu\}_n$ ppz_n in Acetone d_6 with a predicted structure.

The expected percentage of the mixed metal Ag and Cu in $\{[3,5\text{-}(CF_3)_2Pz]AgCu\}_n$ ppz_n is around 20%. TGA (Q50 V6.7) analysis in figure 53 shows that 80.83% weight loss of the

organic ligands in the $\{[3,5\text{-}(CF_3)_2Pz]AgCu\}_n$ ppz_n. It indicates that Ag/Cu mixed-metal composition is left from the remaining percentage of 19.27%, which supports our expectations. The IR spectra for $\{[3,5\text{-}(CF_3)_2Pz]AgCu\}_n$ ppz_n , shown in figure 55, confirms the presence of the ligands (Pz, ppz) in the product.

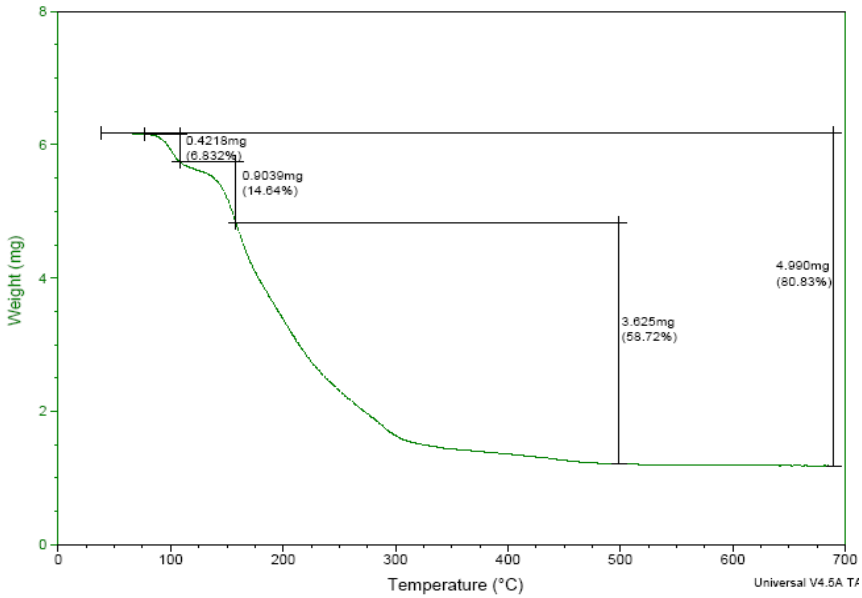

Fig. 53 TGA (Q50 V6.7) analysis of $\{[3,5\text{-}(CF_3)_2Pz]AgCu\}_n$ ppz_n.

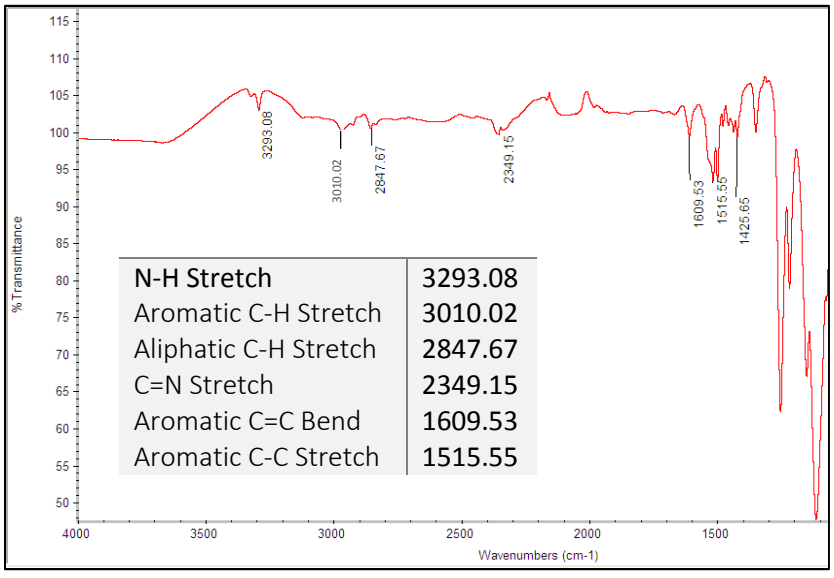

Fig. 54 FT-IR spectrum of $\{[3,5\text{-}(CF_3)_2Pz]AgCu\}_n$ ppz_n

2.6. Results and discussion of mixed ligand complexes

Mixed ligand complex: $\{[3,5\text{-}(CF_3)_2Pz]Ag\}_2$ bpp/bpe was prepared by treatment of trinuclear silver (I) complex with mixing a slight molar excess of the corresponding linear bridging diimine ligands: 4,4′-trimethylenedipyridine (bpp) and 1,2-bis(4-pyridyl) ethylene (bpe) in dichloromethane. It was obtained in high yields (>80%). Mixed ligand complex is air stable crystalline solid. It is partially soluble in organic solvents such as acetonitrile, acetone and tetrahydrofuran but completely soluble after sonication and filteration. We could get crystal structure from $\{[3,5\text{-}(CF_3)_2Pz]Ag\}_2$ bpp/bpe, but we found that it has the same crystal structure of a previous product; $\{[3,5\text{-}(CF_3)_2Pz]Ag\}_2$bpp. We were able to characterize the mixed ligand complex $\{[3,5\text{-}(CF_3)_2Pz]Ag\}_2$ bpp/bpe. It has the same ^{1}HNMR spectroscopy, FT-IR spectroscopy, absorption spectroscopy and TGA as $\{[3,5\text{-}(CF_3)_2Pz]Ag\}_2$bpp. Additionally, it has the same photoluminescence spectra as the product $\{[3,5\text{-}(CF_3)_2Pz]Ag\}_2$bpp at RT and 77K.

CHAPTER III

CONCLUSION

In summary, we were able to synthesize various silver (I) and copper (I) complexes conveniently from cyclic trinuclear Ag(I) and Cu(I) pyrazolate complexes with several bridging diimines. We were able to characterize them using X-ray crystallography, photoluminescene, ^{1}HNMR, IR, TGA, and UV/VIS spectrometry.

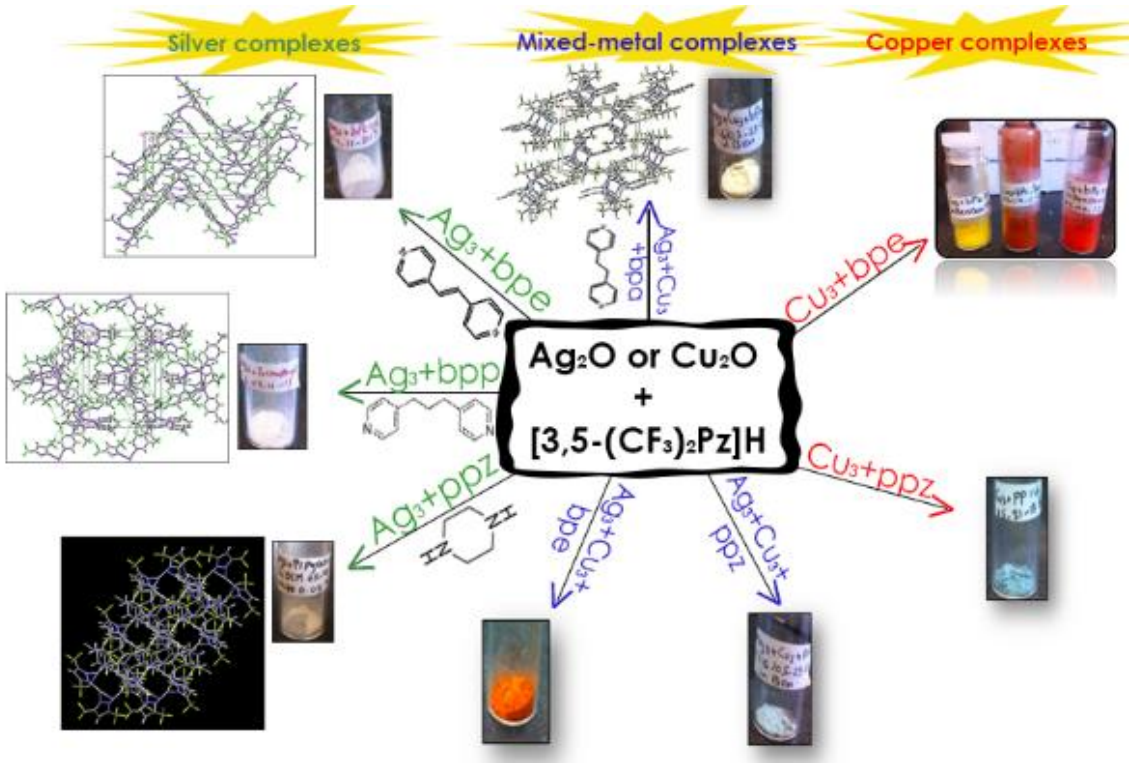

Fig. 55 Schematic representation and illustration of synthetic routes and coordination of copper (I) and silver (I) to different ligands.

Based on all the crystal structures that we obtained, {[3,5-$(CF_3)_2$Pz]Ag}$_2$bpp, {[3,5-$(CF_3)_2$Pz]Ag}$_2$bpe, {[3,5-$(CF_3)_2$Pz]Ag}$_4$ppz, and {[3,5-$(CF_3)_2$Pz]AgCu}$_2$bpa$_2$, we found that pyridine-based diimine could break down the cyclic trinuclear unit and form 3- or 4-coordinate dinuclear units. Since ligands chosen are pyridine-based diimine linkers, the bridge linking the pyridyl groups plays a significant role in the overall ligand size, the geometry and the intermetallic distances formed by the overall complex and the photophysical properties of the complexes.

By comparing the silver complexes, we found that the size of the porosity in the packed structures increases by increasing the length of the bridge linking the pyridyl groups. {[3,5-$(CF_3)_2$Pz]Ag}$_2$bpe with a conjugated linker (shown in figure 20) has smaller porosity than {[3,5-$(CF_3)_2$Pz]Ag}$_2$bpp with propane linker (shown in figures 13). The packing of {[3,5-$(CF_3)_2$Pz]Ag}$_4$ppz with unconjugated bridging ligand (ppz) (shown in gigure 25) shows extended chains with small porosity. The porosity can be functionalized for metal organic frameworks (MOFs) to be used in gas storage, such as hydrogen.

By comparing the copper complexes, we can conclude that increasing the conjugation and decreasing the length of the bridge linking the pyridyl groups increase the stability of the copper complexes. For example, {[3,5-$(CF_3)_2$Pz]Cu}$_n$bpe$_n$ is more stable than {[3,5-$(CF_3)_2$Pz]Cu}$_n$ppz$_n$ and {[3,5-$(CF_3)_2$Pz]Cu}$_n$bpa$_n$ (synthesized by a previous work in our lab [48]).

Different concentrations of $\{[3,5\text{-}(CF_3)_2Pz]Cu\}_n bpe_n$ (1:1), (1:2), (1:6) present different colors (yellow, orange, red), respectively, while $\{[3,5\text{-}(CF_3)_2Pz]Ag\}_2 bpe$ is a white product. The deep color formation tendencies are based on two factors. The first factor is the metal effect. Excited state energy levels are lower for Cu than Ag, leading to red-shifted electronic transitions. The second factor is the ligand effect. Infinite conjugation of unsaturated ligand functionalities (C=N; C=C; N=N) with M centers leads to drastic red shifts in absorption color.

Regarding the photophysical properties, coordination of monovalent silver (I) to a bridging ligand, (4,4′-trimethylenedipyridine)(bpp), results in a compound with interesting tunable photophysical properties. The RT photoluminescence (PL) of the complex with a propane linker exhibited green luminescence with emission being red shifted as the temperature decreases due to narrowing the bandgap as the temperature decreased, while increasing the intensity is due to the non-radiative relaxation. Figures 14 and 15 illustrate the tunable RT and 77K emission at 490nm and 520nm respectively. By looking at this coordination, the emission might be attributed mostly to the Ag….Ag interactions. As seen from the data presented in tables 1 and 3, the dimer of $\{[3,5\text{-}(CF_3)_2Pz]Ag\}_2 bpp$ has shorter Ag….Ag contact (3.3064 Å) than dimers of $\{[3,5\text{-}(CF_3)_2Pz]Ag\}_4 ppz$ (3.2664 Å). Conversely, the dimer of $\{[3,5\text{-}(CF_3)_2Pz]Ag\}_2 bpe$ has no Ag….Ag contact.

Additionally, intense phosphorescence (shown in figures 41 and 42) of a mixed metal complex,$\{[3,5\text{-}(CF_3)_2Pz]AgCu\}_2 bpa_2$, was achieved upon introducing the unsaturated diimine bridging ligand, 1,2-bis(4-pyridyl)ethane (bpa), to the multiple trinuclear coinage

metal azolates. The RT photoluminescence (PL) of the complex with an ethane linker exhibited yellow-green luminescence with emission being red shifted as the temperature decreases probably due to narrowing the bandgap as the temperature decreased, while increasing the intensity is probably due to the non-radiative relaxation. Figures 41 and 42 illustrate the tunable RT and 77K emission at 558nm and 570nm respectively. The crystal structure for the mixed metal complex shows 4-coordinate silver and copper interconnected dimeric units with 0.70 and 1.3 probabilities for silver and copper respectively.

By comparing the properties of the compounds, $\{[3,5\text{-}(CF_3)_2Pz]AgCu\}_2bpa_2$,$\{[3,5\text{-}(CF_3)_2Pz]Ag\}_2bpa$ [48] and $\{[3,5\text{-}(CF_3)_2Pz]Cu\}_nbpa_n$ [48], we can conclude that the properties of mixed metal complex with bpa linker are closer to the properties of the copper complex with the same ligand than the silver complex, including the photophysical properties, because, as shown in table 4, $\{[3,5\text{-}(CF_3)_2Pz]AgCu\}_2bpa_2$ has much probability of copper (1.3) than silver (0.7). We can also conclude that the properties of the mixed metal complex with bpe linker are closer to the properties of the copper complex with the same ligand than the silver complex, because the mixed metal complexes $\{[3,5\text{-}(CF_3)_2Pz]AgCu\}_2bpa_2$ and the copper complex $\{[3,5\text{-}(CF_3)_2Pz]Cu\}_nbpa_n$ are colored products and have yellow luminescence unlike the silver product $\{[3,5\text{-}(CF_3)_2Pz]Ag\}_2bpa$ that has no luminescence and has white color.

The silver polymeric structures exhibit interesting chemical and physical properties that merit further studies. Interesting applications, including use in electronic devices (OLEDs

or solar cells) and gas storage, might be afforded due to interesting optoelectronic or porous properties that can be further tuned upon other structural variations (ongoing).

We made several attempts to re-crystallize the complexes, $\{[3,5\text{-}(CF_3)_2Pz]Cu\}_n bpe_n$, $\{[3,5\text{-}(CF_3)_2Pz]Cu\}_n ppz_n$, $\{[3,5\text{-}(CF_3)_2Pz]AgCu\}_n bpe_n$ and $\{[3,5\text{-}(CF_3)_2Pz]AgCu\}_n ppz_n$, using different solvents and different techniques. However, due to the high sensitivity of copper (I) complexes, we were not able to obtain the crystal structures for those complexes. The research on finding the crystal structure for copper complexes and other mixed metal complexes is still continuous and merit future consideration.

REFERENCES

1- (a) Crespo, O.; Gimeno, M. C.; Laguna, A.; Larraz, C. Z. *Naturforsch*. **2009**, *64b*, 1525 – 1534 S.
(b) Roundhill, D.M.; Fackler, J. P. Jr. *Plenum Publishing Corp., New York*, **1999**, pp. 29.
(c) Yam, V.W.W.; Lo, K. K.W. *Chem. Soc. Rev*. **1999**, *28*, 323.
(d) Fu, W.-F.; Chan, K.-C.; Cheung, K.-K.; Che, C.-M. *Chem. Eur. J*. **2001**, *7*, 4656.
(e) Yam, V.W.W.; Lo, K.K.W.; Fung, W.K.M.; Wang, C.R. *Coord*. *Chem.Rev.* **1998**, *171*, 17.
(f) Vogler, A.; Kunkely, H. *Coord. Chem. Rev*. **2001**, *219*, 489.
(g) Ford, P.C.; Cariati, E.; Bourassa, J. *Chem. Rev*. **1999**, *99*, 3625.
(h) Chen, C.H.; Shi, J. *Coord. Chem. Rev*. **1998**, *171*, 161.

2- (a) Bo Hu, G. G.; Zhang, J., *J. Phys. Chem. A.* **2007**, *111*, 4965-4973
(b) Baldo M.A.; Thompson, M. E.; Forrest, S.R., *Pure Appl. Chem*. **1999**, *71*, 2095.
(c) Evans, R.C.; Douglas, P.; Wiscom, C. J. *Coord. Chem. Rev.* **2006**, *250*, 2093.

3- Hayashi, A.; Olmstead, M. M.; Attar, S.; Balch, A. L. *J. Am. Chem. Soc.* **2002**, *124*, 5791.

4- (1) (a) Baba, A. I.; Shaw, J. R.; Simon, J. A.; Thummel, R. P.; Schmehl, R. H. *Coord. Chem. Rev*. **1998**, *171*, 43.
(b) Armaroli, N. *Chem. Soc. Rev*. **2001**, *30*, 113.
(c) Hay, P. J. *J. Phys. Chem. A*. **2002**, *106*, 1634.
(d) Chou, P.-T.; Chi, Y. *Chem.—Eur. J*. **2007**, *13*, 380.
(e) Vlcek, A., Jr. *Top. Organomet. Chem*. **2010**, *29*, 73.
(f) Hsu, C.-W.; Lin, C.-C.; Chung, M.-W.; Chi, Y.; Lee, G.-H.; Chou, P.-T.; Chang, C.-H.; Chen, P.-Y. *J. Am. Chem. Soc*. **2011**, *133*, 12085–12099

5- (a) Abdou, H. E.; Mohamed, A. A.; Fackler, J. P. Jr. *Inorg. Chem*. **2007**, *46*, 141-146

(b) Schmidbaur, H. Ed. Gold: Progress in Chemistry, Biochemistry and Technology; John Wiley & Sons: *Chichester, U.K.*, **1999**.

6- Burini, A.; Mohamed, A. A.; Fackler, J. P. Jr. *Comments on Inorganic Chemistry*. **2003**, *24*, 253–280.

7- Burini, A.; Bravi, R., Fackler, J. P., Jr.; Galassi, R., Grant, T. A.; Omary, M. A.; Pietroni, B. R.; Staples, R. *J. Inorg. Chem*. **2000**, *39*, 3158.

8- Burini, A.; Fackler, J. P., Jr.; Galassi, R.; Pietroni, B. R.; Staples, R. J. *J. Chem. Soc., Chem. Commun*. **1998**, *95*.

9- Murray, H. H.; Raptis, R. G.; Fackler, J. P. JR. *Inorg. Chemn*. **1988**, *27*, 26

10- Trofimenko, S.; Prog. *Inorg. Chem*. **1986**, *34*, 115.

11- Yang, G.; Raptis, R.G. *Inorg. Chem*. **2003**, *42*, 261.

12- Omary, M. A.; Rawashdeh-Omary, M. A.; Gonser, M. W. A.; Elbjeirami, O.; Grimes, T.; Cundari, T. R.; Diyabalanage, H. V. K.; Gamage, C. S. P.; Dias, H. V. R. *Inorg. Chem*. **2005**, *44*, 8200-8210.

13- Dias, H.V. R.; Polach, S. A.; Wang, Z. *Journal of Fluorine Chemistry*. **2000**, *103*, 163±16

14- Ehlert, M. K.; Rettig, S. J.; Storrr, A.; Thompson, R. C.; Trotter. J. *Can. J. Chem*. **1990**, *68*, 1444.

15- (a) Adachi, C.; Baldo, M. A.; Forrest, S. R. *J. Appl. Phys*. **2000**, *87*, 8049.
(b) Zhang, J.; Kan, S.; Ma, Y.; Shen, J.; Chan, W.; Che, C. *Synth Met.* **2001**, *121*, 1723.
(c) Grushin, V. V.; Herron, N.; LeCloux, D. D.; Marshall, W. J.; Petrov, V. A.; Wang, Y. *Chem. Commun*. **2001**, *16*, 1494.
(d) Omary, M. A.; Rawashdeh-Omary, M. A.; Diyabalanage, H. V.K.; Dias, H. V. R. *Inorg. Chem*. **2003**, *42*, 8612.
(e) Dias, H. V. R.; Lu, H.-L. *Inorg. Chem*. **1995**, *34*, 5380.
(f) Dias, H. V. R.; Kim, H.-J.; Lu, H.-L.; Rajeshwar, K.; de Tacconi, N. R.; Derecskei-Kovacs, A.; Marynick, D. S. *Organometallics* **1996**, *15*, 2994.
(g) Dias, H. V. R.; Jin, W. J. *Am. Chem. Soc.* **1995**, *117*, 11381.
(h) Dias, H. V. R.; Jin, W. *Inorg. Chem.* **1996**, *35*, 3687.

(i) Dias, H. V. R.; Lu, H.-L.; Kim, H. J.; Polach, S. A.; Goh, T. K. H.H.; Browning, R. G.; Lovely, C. *J. Organometallics* **2002**, *21*, 1466.

16- (a) Dias, H. V. R.; Diyabalanage, H. V. K.; Rawashdeh-Omary, M. A.; Franzman, M. A.; Omary, M. A. *J. Am. Chem. Soc*.**2003**, *125*, 12072.
(b) Dias, H. V. R.; Diyabalanage, H. V. K.; Eldabaja, M. G.; Elbjeirami, O.; Rawashdeh-Omary, M. A.; Omary, M. A. *J. Am. Chem. Soc*.**2005**, *127*, 7489.

17- Dias, H. V. R; Gamage, C. S; Kelter, J; Diyabalanage, H. V. K; Omari, I; Eyobo, Y; Dias, N. R; Roehr, N; McKinney, L; Poth, T. *Inorg. Chem*. **2007**, *46*, 8, 2979

18- (a) Haneline, M. R.; Tsunoda, M.; Gabbaı¨, F. P. *J. Am. Chem. Soc.* **2002**, *124*, 3737.
(b) Omary, M. A.; Kassab, R. M.; Haneline, M. R.; Elbjeirami, O.;Gabbaı¨, F. P. *Inorg. Chem.* **2003**, *42*, 2176.
(c) Dias, H. V. R.; Diyabalanage, H. V. K. *Polyhedron* **2006**, *25*, 1655.
(d) Grimes, T.; Omary, M. A.; Dias, H. V. R.; Cundari, T. R. *J. Phys.Chem. A* **2006**, *110*, 5823.
(e) Adachi, C.; Baldo, M. A.; Forrest, S. R. *J. Appl. Phys*. **2000**,*87*, 8049.
(f) Zhang, J.; Kan, S.; Ma, Y.; Shen, J.; Chan, W.; Che, C. *Synth.Met.* **2001**, *121*, 1723.
(g) Grushin, V. V.; Herron, N.; LeCloux, D. D.;Marshall, W. J.; Petrov, V. A.; Wang, Y. *Chem. Commun*. **2001**, *16*, 1494.
(h) Omary, M. A.; Rawashdeh-Omary, M. A.; Diyabalanage, H. V. K.; Dias, H. V. R. *Inorg. Chem.* **2003**, *42*, 8612.

19- Omary, M. A.; Rawashdeh-Omary, M. A.; Diyabalanage, H. V. K.; Dias, H. V. R.. *Inorg. Chem.* **2003**, *42*, 8612-8614

20- Sun, D.; Yuan, S.; Wang, H.; Lu, H. F.; Feng, S. Y.; Sun, D. F. *Chem Commun (Camb).* **2013**, *49*, 6152-4.

21- Pan, Q.-J.; Guo, Y.-R.; Zhang, H.-X. *Organometallics*. **2010**, *29*, 3261–3270, 3261

22- Chandrasekhar, V.; Hajra, T.; Bera, J. K.; Wahidur Rahaman, S. M.; Satumtira, N. T.; Elbjeirami, O.; Omary, M. A. *Inorg. Chem*. **2011.**

23- Vickery, J. C.; Olmstead, M. M.; Fung, E. Y.; Balch, A. L. Angew. *Chem., Int. Ed. Engl.* **1997**, *36*, 1179.

24- (a) Dias, H. V. R.; Diyabalanage, H. V. K. *Polyhedron* **2006**, *25*, 1655.
(b) Dias, H. V. R.; Diyabalanage, H. V. K.; Rawashdeh-Omary,M. A.; Franzman, M. A.; Omary, M. A. *J. Am. Chem. Soc*. **2003**, *125*,12072.
(c) Dias, H. V. R.; Diyabalanage, H. V. K.; Eldabaja, M. G.;Elbjeirami, O.; Rawashdeh-Omary, M. A.; Omary, M. A. *J. Am. Chem.Soc*. **2005**, *127*, 7489.
(d) Grimes, T.; Omary, M. A.; Dias, H. V. R.; Cundari, T. R. *J. Phys.Chem. A* **2006**, *110*, 5823.
(e) Omary, M. A.; Rawashdeh-Omary, M. A.; Diyabalanage, H. V.K.; Dias, H. V. R. *Inorg. Chem*. **2003**, *42*, 8612.
(f) Dias, H. V. R.; Polach, S. A.; Wang, Z. *J. Fluorine Chem*. **2000**,*103*, 163.

25- Mohammed, A. A.; Galasi, R.; Papa, F.; Burini, A.; Fackler, J. P. Jr. *Inorganic Chem*. **2006**, *45*, 19, 7771

26- Mohammed, A. A.; Burini, A.; Fackler, J. P. Jr. *J. Am. Chem. Soc*. **2005**, *127*, 5012-5013

27- Omary, M. A; Rawashdeh-Omary, M. A; Gonser; Elbjeirami, O; Grimes, T; Cundari, T. R; Diyabalanage, H. V. K; Gamage, C. S P; Dias, H. V. K. *Inorg. Chem*. **2005**, *44*, 23

28- Fernandez, E. J.; Lagunab, A and Lopez-de-Luzuriaga, *J.M. Gold Bulletin*. **2001**, *34*, 1.

29- Mohammed, A. A.; Galasi, R.; Papa, F.; Burini, A.; Fackler, J. P. Jr. *Inorganic Chem.* **2006**, *45*(19), 7771.

30- Moher, F. Gold Chemistry. *Wily-VCH*, **2009**. Print

31- Usón, R.; Laguna, A.; Laguna, M.; Manzano, B.R.; Jones, P.G.; Sheldrick, G.M. *Journal of the Chemical Society, Dalton Transactions*, **1984**, *2*, 285

32- Lopez, N.; Norskov, J. K. *J. Am. Chem. Soc*. **2002**, *124*, 11262

33- Roundhill, D. M.; Fackler, J. P. Jr. *Plenum Press: New York*, **1999**.

34- Abdou, H. E.; Mohamed, A. A.; Fackler, J. P. Jr. *Inorg. Chem*. **2007**, *46*, 141-146

35- Hettiarachchi, C. V.; Rawashdeh-Omary, M. A.; Korir, D.; Kohistani, J.; Yousufuddin, M.; Dias, H. V. R. *Inorg. Chem*. **2013**, *52*, 13576−13583

36- Omary, M. A.; Elbjeirami, O.; Gamage, C. S. P.; Sherman, K. M.; Dias, H. V. R. *Inorg. Chem*. **2009**, *48*, 1784−1786.

37- Rawashdeh-Omary, M. A.; Rashdan, M. D.; Dharanipathi, S.; Elbjeirami, O.; Ramesh, P.; Dias, H. V. R. *Chem. Commun*. **2011**, *47*,1160−1162.

38- (a) Ma, S.; Zhou, H.-C. *Chem. Commun.* **2010**, *46*, 44–53
(b) Long, J. R.; Yaghi, O. M. *Chem. Soc. Rev.,* **2009**, *38*, 1213–1214.
(c) Lee, J.; Farha, O. K.; Roberts, J.; Scheidt, K. A.; Nguyen, S. T.; Hupp, J. T. *Chem. Soc. Rev*., **2009**, *38*, 1450–1459.
(d) Kurmoo, M. *Chem. Soc. Rev.,* **2009**, *38*, 1353–1379.
(e) Allendorf, M. D.; Bauer, C. A.; Bhakta, R. K.; Houk, R. J. T. *Chem. Soc. Rev*., **2009**, *38*, 1330–1352.
(f) Morris, R. E.; Wheatley, P. S. *Chem., Int. Ed*., **2008**, *47*, 4966–4981.
(g) Li, J.-R.; Kuppler, R. J.; Zhou, H.-C. *Chem. Soc. Rev*., **2009**, *38*, 1477–1504.
(h) Yaghi, O. M.; O'Keeffe, M.; Ockwig, N. W.; Chae, H. K.; Eddaoudi, M.; Kim, J. *Nature*, **2003**, *423*, 705–714.
(i) M. O'Keeffe, *Chem. Soc. Rev*., **2009**, *38*, 1215–1217.
(j) Eddaoudi, M.; Kim, J.; Rosi, N.; Vodak, D.; Wachter, J.; O'Keeffe, M.; Yaghi, O. M. *Science*, **2002**, *295*, 469–472.
(k) Fe´rey, G. *Chem. Soc. Rev*., **2008**, *37*, 191–214.
(l) Suh, M. P.; Cheon, Y. E.; Lee, E. Y. *Coord. Chem. Rev*., **2008**, *252*, 1007–1026.
(m) Kitagawa, S.; Noro, S.-i.; Nakamura, T. *Chem. Commun*.,**2006**, 701–707.
(n) Kitagawa, S.; Matsuda, R. *Coord. Chem. Rev*., **2007**, *251*, 2490–2509.

39- Tranchemontagne, D. J.; Hunt, J. R.; Yaghi, O. M. *Tetrahedron*, **2008**, *64*, 8553–8557.

40- Furukawa et al. *Science.* **2010**, *329*, 424-4284

41- Yaghi, O. M.; Hailian, L.; Davis, C.; Richardson, D.; Groy, T. *Acc. Chem. Res*. **1998**, *31*, 474-484.

42- Ghosh, S. K.; Ribas, J.; Bharadwaj, P. K. *Crystal Growth & Design.* **2005**, *5*, 2, 623-629.

43- Murray, L. J.; Dincă, M.; Long, J. R. *Chem. Soc. Rev*. **2009**, *38*, 1294-1314.

44- Janiak, C.; Vieth, J. K. *New J. Chem*. **2010**, *34*, 2366–2388.

45- Zhu, J.; Hsu, C.; Yu, Z.; Fan, S.; Cui, Y. *Nano Lett*. **2010**, *10*, 1979–1984.

46- Matt Law, L.; Greene, J. C.; Johnson, R. S.; Yang, P. *Nature Materials.* **2005**, *4*.

47- Omary, M. Organic Light-Emitting Diodes from Homoleptic Square Planer Complexes. Patent US 8,580,397 B2, November 12, **2013**.

48- Kolailat, S.; Rawashdeh-Omary, M. A. Unpublished results.

49- SHELXTL (Version 5.1), *Bruker Analytical X-ray Systems, Inc., Madison, WI, USA*, **1997**.

50- (a) Oregan, B.; Gratzel, M. *Nature*, **1991**. 353(6346): p. 737-740.
(b) Green, M.A., et al., *Progress in Photovoltaics*, **2009**. *17*(1): p. 85-94.